rijksinstituut voor volksgezondheid en milieuhygiëne, bilthoven
koninklijk nederlands meteorologisch instituut, de bilt

Description of the RIVM/KNMI puff dispersion model

G. H. L. Verver
F. A. A. M. de Leeuw
H. J. van Rheineck-Leyssius

KNMI
publicatie 177

RIVM
rapport
222501001

gezamenlijk knmi/rivm project

1990

rijksinstituut voor volksgezondheid en milieuhygiëne, bilthoven
koninklijk nederlands meteorologisch instituut, de bilt

Description of the RIVM/KNMI puff dispersion model

G. H. L. Verver [+]
F. A. A. M. de Leeuw [*]
H. J. van Rheineck-Leyssius [*]

KNMI
publicatie 177

RIVM
rapport
222501001

gezamenlijk knmi/rivm project

knmi De Bilt [+]
rivm Bilthoven [*] 1990

contents

Samenvatting

In dit rapport wordt het RIVM/KNMI puffmodel beschreven. Het model is een aangepaste versie van PUFF (Van Egmond and Kesseboom, 1983). Het is bedoeld voor operationeel gebruik op het KNMI en het RIVM in geval van een calamiteit waarbij giftige en/of radioactieve gassen of deeltjes in de atmosfeer terecht komen. Het model gebied wordt beperkt door de meteorologische invoer; in de operationele toepassing omvat het model (bijna) geheel Europa.

De belangrijkste processen die door het model worden beschreven zijn: relatieve diffusie door wind schering en turbulentie, advectie als functie van plaats en tijd, de dagelijkse gang van de grenslaag dikte en stabiliteit, droge en natte depositie en lineaire chemische omzetting of radioactief verval.

Invoer velden voor het model zijn: horizontale wind (elke 3 of elke 6 uur, op 2 of 3 niveau's), neerslag (elke 3 uur; optioneel) en de dikte van de grenslaag (elke 3 uur; optioneel). De meteorologische velden kunnen zowel analyses zijn als prognoses.

De bron wordt beschreven door een effectieve bronhoogte en een emissie sterkte als functie van de tijd.

Het model berekent velden van grondconcentraties en droge en natte depositie als functie van tijd.

Het RIVM/KNMI puffmodel is getest met de verspreiding van Cs-137 en I-131 over Europa na het Chernobyl ongeval (april-mei, 1986). De verspreiding gedurende een periode van 10 dagen is gesimuleerd, en de resultaten zijn vergeleken met metingen.

De aankomsttijden worden goed gereproduceerd, voor de meeste stations binnen een nauwkeurigheid van 6 uur. De concentraties komen tot op een orde van grootte overeen.

Summary

In this paper the RIVM/KNMI puff dispersion model is described. The model is an adapted version of PUFF (Van Egmond and Kesseboom, 1983). It is intended for operational use at KNMI and RIVM in case of an accidental release of (toxic or radioactive) gases or particles into the atmosphere. The area covered by the model is restricted by the meteorological input that is available; the operational version will cover most of Europe.

The main processes accounted for by the model are: relative diffusion by wind shear and turbulence, advection as a function of space and time, the diurnal cycle of boundary layer height and stability, dry and wet deposition and linear chemical transformation or radioactive decay.

Input fields for the model are: horizontal wind (every 3 or 6 hours, on 2 or 3 levels), precipitation data (every 3 hours; optional) and height of the boundary layer (or mixed layer; every 3 hours; optional). The meteorological data used may be either analyses or prognostic fields. The source is defined by an effective emission height and the source strength as a function of time.

The model calculates fields of concentrations near the surface and dry and wet depositions as a function of time.

The RIVM/KNMI puffmodel is tested on the Cs-137 and iodine-131 dispersion over Europe during the Chernobyl episode (April and May 1986). A ten day period is simulated and results are compared with measurements.

Arrival times of the material are simulated well, in most cases within 6 hours accuracy. The observed air concentrations and model outcome show a reasonable agreement, but may differ an order of magnitude.

1 Introduction and background

On 26 April 1986 a severe accident occurred at the nuclear power plant in Chernobyl. During approximately 11 days large amounts of radioactive material were emitted into the atmosphere. During the days that followed, the contaminants were tracked over Europe by analyses of the meteorological situation and a small number of radioactivity measurements. In the following weeks more measurements became available and dispersion models were used to reconstruct the deposition and concentration patterns over Europe.

The experience during the Chernobyl accident leads to the conclusion that, in an early stage, dispersion models could give valuable estimates of the impact of an accidental release of material into the atmosphere. For this purpose, RIVM and KNMI developed a puff dispersion model. The model is an adapted version of the model PUFF by Van Egmond and Kesseboom (1983).

The aim of the model is to calculate concentrations and depositions of hazardous material that is released accidently into the atmosphere. The model area may, in principle, be chosen freely. However, most of the calculations will be performed on a European scale (ca. 3000*3000 km), or on the scale of The Netherlands and surroundings (ca. 400*400 km).

Model results may be used to estimate the pollutant exposure of the population directly by air or indirectly e.g. through the food chain. The model produces valuable input to models describing the exposure pathway to estimate the dose.

Processes accounted for by the dispersion model are:

-1- relative diffusion by turbulence and wind shear,
-2- advection of material dependent on height,
-3- dry deposition (dependent on stability) and wet deposition,
-4- linear chemical transformation or radioactive decay (dc/dt=constant*c)
-5- the diurnal cycle of stability and mixing height.

The quality of the dispersion calculations depends heavily on the quality of the meteorological input data. The residence time of the material over Europe may be several days, during which the meteorological situation may change considerably. Two models generate the necessary meteorological input for the dispersion model: -1- the KNMI Fine Mesh Limited Area Model (KNMI FM-LAM), and -2- The ECMWF global model. Input may be either analysed data or prognostic fields. Using these meteorological models, the dispersion model is able to calculate the situation effectively 96 hours ahead.

In most applications, the model will have only a single source of one or two pollutants. With respect to computer resources the Lagrangian description is therefore appropriate. Also, near the source, proper detail is attained and effects of numerical diffusion are avoided. However, nonlinear processes (like more complex chemistry) can not be accounted for by the model.

The emission may either be instantaneous or continuous, with a strength varying in time

In Chapter 2 of this report the mathematical description of the model is given. Chapter 3 defines the meteorological input data of the model. Chapter 4 gives results of the model as applied to the Chernobyl accident, and a comparison with measurements is made. The technical details of the implementation and software will be given in a KNMI technical report and a RIVM report.

2 Description of the dispersion model

An emission from a point source is divided into a number of Gaussian shaped puffs containing mass $M=Q.\Delta t$, where Q is the source strength (emission units per second) and Δt is the timestep of the model, which is one hour in the version described here. In case of an instantaneous emission, only one puff is released. The source strength Q is input to the model, and may be updated every hour.

The mass of each puff is distributed over two layers, the mixed layer and the reservoir layer (figure 1; sections 2.1 and 2.2). The presence of two layers in this model allows descriptions of the process of fumigation and the transport of pollutants at higher altitudes, decoupled from the surface.

Within the mixed layer, turbulence is generated by wind shear and/or buoyancy, and material will be dispersed rapidly. The turbulence intensity within the reservoir layer is absent or very small, and material diffuses only very slowly in the vertical direction (section 2.3). The effects of wind shear on horizontal puff growth is discussed in section 2.4.

The advection velocity is determined by interpolation of the wind vectors to the mass-centre of the puff. The diurnal cycle of mixing height causes a material flux between both layers (section 2.5) which, in conjunction with a different advection in these layers, enhances the horizontal spread of material (e.g. McNider, 1988). To take into account this effect of wind shear on dispersion, a procedure is developed to split a puff into two separate puffs that will be advected separately, one in the mixed layer, and one in the reservoir layer (section 2.7).

The mass in the mixed layer is affected by the dry deposition process; wet deposition affects masses in both layers (sections 2.8 and 2.9). Radioactive decay or chemical transformation affects the mass in both layers (section 2.10).

Some processes are not taken into account by the model. In the first place these are physical phenomena not resolved by the model, like convective clouds, local effect on the wind fields and convective precipitation. Since advection is calculated using only the horizontal components of the wind, large-scale subsidence or upward movements are also not taken into account. However, these large-scale processes do affect the boundary layer height used in the model, since it is derived from the meteorological model that at least partly resolves these processes.

The formulation of the dispersion model restricts its applicability to transport times more than approximately one hour and distances more than ~30km.

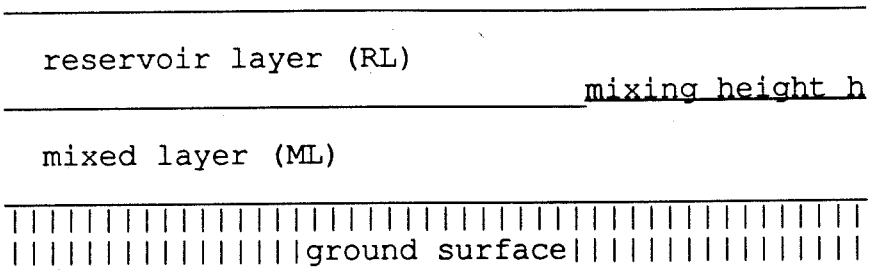

Figure 1 Layers of the RIVM/KNMI puff dispersion model

2.1 Definition of layers

The height of the turbulent mixed layer in the model is a function of time in order to account for the diurnal cycle caused by insolation. Local differences in surface characteristics, like roughness, humidity, albedo and differences in insolation caused by cloud cover, make the mixing height a function of position also. These differences will be most apparent near a land/sea transition. Above land, the height of the mixed layer is typically 100m during the night and 1500m during daytime.

There is no rigid upper limit to the height of the reservoir layer. It is determined by the maximum height to which material of a single puff is dispersed. Therefore,the upper boundary of the reservoir layer depends on the vertical diffusion coefficient for material in the reservoir layer, and, if the emission takes place above the mixed layer, also on the effective emission height.

Figures 2a and b show examples of layer heights and concentration profiles as a function of time.

a

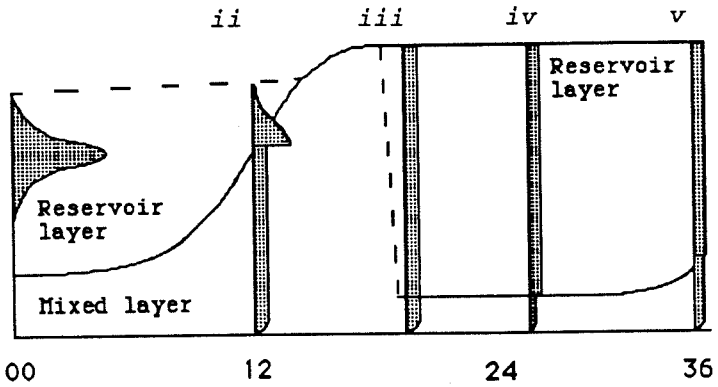

i- Material is directly emitted into the reservoir layer (H>h). The vertical profile is Gaussian.

ii- The dispersion coefficient of the mass in the reservoir layer is changed only slightly. A part of the material is entrained into the mixed layer due to a rise of the mixing height. In the mixed layer a uniform concentration profile is assumed. Close to the surface a concentration gradient is introduced by dry deposition.

iii- At the time the maximum mixing height is reached, all material is entrained and uniformly mixed in the mixed layer. When at the end of the day turbulence decays, this layer is split into a reservoir layer having a uniform concentration profile and a shallow stable nighttime boundary layer.

iv - During the night the concentration in the mixed layer will reduce due to dry deposition.

v- After a break up of the stable boundary layer during the morning hours, material from the reservoir layer is entrained into the mixed layer and rapidly mixed to the ground

b

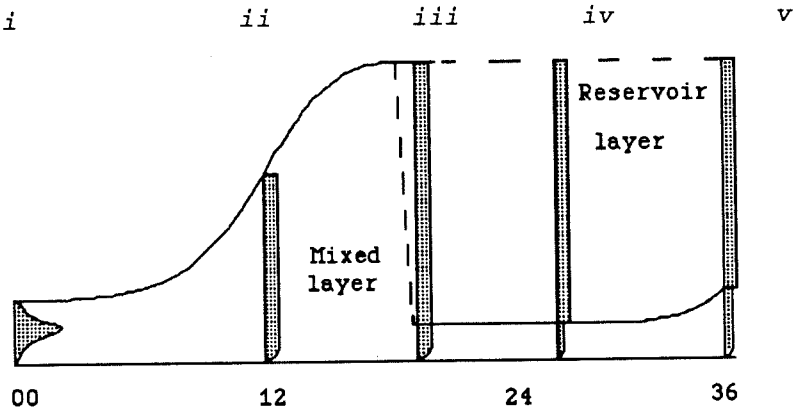

i- Material is emitted into the mixed layer (H<h).

ii- After a few hours the material is well mixed, and a uniform concentration profile is assumed. Close to the surface a concentration gradient is introduced by dry deposition.

iii- The mixed layer is split into a stable nighttime boundary layer, and a reservoir layer.

iv - During the night the concentration in the mixed layer will reduce due to dry deposition.

v - After the break up of the stable boundary layer during the morning hours, material from the reservoir layer is entrained into the mixed layer and rapidly mixed to the ground

Figure 2a and b
Two examples of layer heights and vertical concentration profiles as a function of time.

2.2 Description of the puffs

The size of the puffs is characterized by two quantities, the horizontal dispersion coefficient σ_r and the vertical dispersion coefficient σ_z. The horizontal concentration distribution is assumed to be Gaussian and aximetric, the vertical concentration profile is either uniform, when the material is vertically well mixed, or Gaussian with corrections that account for the presence of the ground and the inversion above. Near the ground, the profiles are corrected for dry deposition.

-Mixed Layer-
The concentration within the mixed layer is described by the formula (e.g., Turner, 1970):

$$c(r,z,H) = \frac{M_{ML}}{(2\pi)^{3/2}\sigma_r^2\sigma_z} \cdot \exp\left[-\frac{r^2}{2\sigma_r^2}\right] \cdot \left\{ \exp\left[-\frac{(z-H)^2}{2\sigma_z^2}\right] + \right.$$

$$\text{(term A)} \qquad \exp\left[-\frac{(z+H)^2}{2\sigma_z^2}\right] \quad +$$

$$\text{(term B)} \qquad \exp\left[-\frac{(z+2h-H)^2}{2\sigma_z^2}\right] \quad +$$

$$\text{(term C)} \qquad \left. \exp\left[-\frac{(z+2h+H)^2}{2\sigma_z^2}\right] \right\} \qquad (1)$$

Symbols are explained in the section Notation and Symbols.

Terms A and B are contributions to the concentrations due to reflection of material at the ground surface and at z=h, respectively. Term C is the contribution of material first reflected at the ground surface and then at z=h.

After a few hours (the exact time depends on stability and mixing height), the mass-distribution in the mixed layer is considered vertically homogeneous. In that case, the expression for the concentration distribution around the mass-centre of a puff (eq. 1) simplifies to:

$$\langle c \rangle = \frac{M_{ML}}{2\pi\sigma_r^2 h} \cdot \exp\left[\frac{-r^2}{2\sigma_r^2}\right] \qquad (2)$$

-Concentration near the surface-
The concentration near the surface is affected by dry deposition. Close to the surface a constant flux layer is assumed. The concentration at z=4m is estimated by:

$$c(z=4m) = \langle c \rangle \frac{Vg(z=50m)}{Vg(z=4m)} \qquad (3)$$

where Vg(z) is the deposition velocity (described in section 2.8) and <c> is the concentration obtained by equation (2). It is implicitly assumed that the concentration at z=50m is equal to <c>.

-Reservoir Layer-
When the emission takes place above the mixed layer, the Gaussian shape of the puff within the reservoir layer is described by:

$$c(r,z,H) = \frac{M_{RL}}{(2\pi)^{3/2}\sigma_r^2\sigma_z} \cdot \exp\left[-\frac{(r^2)}{2\sigma_r^2}\right] .\exp\left[-\frac{(z-H)^2}{2\sigma_z^2}\right] \quad (4)$$

where M_{RL} is the mass within the reservoir layer.
In this layer there is very little turbulence, so the vertical dispersion σ_z will barely change.
When the mixing height rises, mass will be transported from the reservoir layer to the mixed layer. It is assumed that this material is instantly and fully mixed in the mixed layer (see figure 2a, stage ii). When at the end of the day the turbulent boundary layer decays and a shallow stable nocturnal boundary layer is formed, a uniform concentration profile remains in the reservoir layer. The concentration in the reservoir layer is then described by:

$$c(r\ ,\ h, h_{old}) = \frac{M_{RL}}{2\pi\sigma_r^2 (h-h_{old})} \cdot \exp\left[-\frac{(r^2)}{2\sigma_r^2}\right] \qquad (5)$$

where h_{old} is the mixing height just before the decay of the daytime boundary layer and h is the actual boundary layer height (see figure 2a and 2b, stage iii).

2.3 Vertical dispersion coefficients

-Mixed Layer-

When a puff is released in the mixed layer, turbulence will spread the material vertically. This growth is estimated by the empirical formula:

$$\sigma_z = ax^b \quad , \tag{6}$$

where x is the length of the trajectory of the puff, and a and b are stability dependent quantities. We used table 1 for the assignment of values for a and b, where the Pasquill stability class was based on the Obukhov length (section 3.4) and the roughness length (Golder, 1972).

Pasquill	a	b
A	0.28	0.90
B	0.23	0.85
C	0.22	0.80
D	0.20	0.76
E	0.15	0.73
F	0.12	0.67

Table 1 Vertical dispersion coefficient parameters a and b in: $\sigma_z = ax^b$ (Pasquill, 1974)

When $\sigma_z > h/\sqrt{12}$ [1], the vertical mass distribution is considered homogeneous over the mixed layer, and eq. (2) is applied.

[1] The dispersion coefficient is defined as:

$\sigma_z^2 \equiv (\overline{c(z)^2} - \overline{c(z)}^2)/(M_{ML})^2$ A vertically fully mixed puff will have:

$$\sigma_z^2 = \frac{1}{h}\int_0^h z^2 dz - \left(\frac{1}{h}\int_0^h z dz\right)^2 = \frac{1}{3}h^2 - \left(\frac{1}{2}h\right)^2 = \frac{1}{12}h^2$$

-Reservoir Layer-
Within the reservoir layer turbulence is almost zero. The vertical dispersion coefficient is calculated by:

$$\sigma_z^2 = 2K_z t \qquad (7)$$

where K_z is set to a very small value: 0.5 m^2/s.

2.4 Horizontal dispersion coefficients

The horizontal dimension of a puff increases due to turbulence and due to shear of the horizontal wind direction and wind speed. In this section first the puff growth due to turbulence is described, then the equations describing the dispersion of material due to wind shear. Very briefly a description is given of dispersion observations by Gifford. After this the model formulation of horizontal dispersion is given.

-Turbulence-
Following Taylor's dispersion theory, the size of a puff will grow due to turbulence initially proportional with time t. When the horizontal size of a puff is much larger than the size of the largest eddies, it will grow proportional with $t^{1/2}$. The distinctions between these regimes is determined by the characteristic timescale of the largest horizontal eddies, the Lagrangian timescale t_{Lh}, defined by:

$$t_{Lh} = \int_0^\infty R(\tau)\, d\tau \ , \qquad (8)$$

where the lagrangian autocorrelation function is usually written as the exponential function $R(\tau) = \exp(-\tau/t_{Lh})$. The horizontal growth rate is written as (e.g. Csanady, 1973):

$$\frac{d\sigma_y^2}{dt} = 2\overline{u_m^2} \int_0^t R_L(\tau)\, d\tau. \qquad (9)$$

For horizontal dispersion a wide range of eddy sizes contributes to dispersion. Unlike vertical eddies, horizontal eddies are not limited by the height of the boundary layer. Therefore, mesoscale and synoptic-scale turbulence of spatial scales up to several hundred kilometers may contribute to horizontal growth. Gifford (1985) cautiously suggests a t_{Lh} somewhere between 40 and 80 hours to explain observational data from the Mt.Isa smelter plume (see figure 3).

-Wind shear-

A second important mechanism for horizontal puff growth is vertical shear of the horizontal wind vector. In this paper this is referred to simply as 'wind shear'.

In the contribution of wind shear to puff growth, three stages may be distinguished. The first stage, immediately after the release from the point source, the cloud will grow in the horizontal direction due to turbulence alone. In stable situations, with strong wind shear, this stage may be absent.

The puff will grow in the vertical direction also, and the the shear of the horizontal wind to which it is exposed starts to contribute to its horizontal spread (stage 2). Expressions have been derived for this contribution by Saffman (1962), Smith (1965), Van Egmond et al. (1982) and Venkatram (1988). They find for a puff growing unbounded in all directions:

$$\frac{d\sigma_x^2}{dt} = c.(\bar{du}/dz)^2.K_z.t^2 \quad \text{for } t \gg t_L \qquad (10)$$

where c is a constant, t_L is the lagrangian timescale for vertical velocities, $\bar{du}/dz$ and the vertical exchange coefficient K_z are constant with height [2]. This stage of puff growth is not taken into account by the puff model, because equation (10) is restricted to a very limited timerange, under most circumstances less than the one hour timestep of the current version of the model.

The rapid growth described by equation (9) will come to an end when the material is fully mixed within the boundary layer (stage 3). The vertical size remains constant, this leads to a diminished growth rate in the horizontal direction. Saffman (1962) derived for this case:

$$\frac{d\sigma_x^2}{dt} = (\bar{du}/dz)^2.h^4/(60.K_z) \qquad (11)$$

According to equation (11), a puff trapped within the mixed layer, grows like the square root of time (in a stationary situation, the right hand side is a constant).

-Observations-

Observations compiled by Gifford (1977) show σ_y^2 proportional to t^3 up to 3000 seconds of travel time. An updated set of observational data (Gifford, 1985) is depicted in figure 3. It shows that for travel times from one hour up to approximately 4 days σ_y^2 is proportional t^2. This is also found by Hanna (1986).

---

[2] Van Egmond et al.(1982) and Venkatram (1988) derive:
$\sigma_y^2 = c'.(\bar{du}/dz)^2.\sigma_z^2.t^2$, which is similar to eq. 10), since for large times $\sigma_z^2 \cong 2K_z t$.

Model calculations by McNider (1988) show that the prolonged linear growth rate found by observations, may also be explained by the diurnal cycle of the boundary layer height in combination with vertical wind shear.

-The model-

In the RIVM/KNMI puff model a simple formulation of the horizontal spread is chosen, keeping in mind the considerations given above. A nearly linear growth of σ_r is found in most observations, even up to 50 kilometers. It may be explained by either the large range of spatial scales of horizontal turbulence (Gifford, 1985) or the diurnal cycle of wind shear in combination with vertical mixing (e.g. Pasquill and Smith, 1983; McNider, 1988). Beyond the spatial range of these observations, the model at least partly resolves the large scale turbulence, due to the puff-projection mechanism described in section 2.7. The model resolves also a part of the effect of wind shear on horizontal dispersion by its two layer structure. Therefore, puffs smaller than approximately the grid spacing will be imposed a linear growth rate, as found by observations and explained by subgrid wind shear and turbulence. Larger puffs will disperse mainly by processes resolved by the model. To account for the contribution of subgrid scale processes, a growth rate like the square root of time is imposed. The interpolation between these regimes is obtained by an equation similar to Taylor's formulation (eq. (9)):

$$\frac{d\sigma_r^2}{dt} = c'' \int_0^t R_*(\tau)\, d\tau \quad , \qquad (12)$$

where $R_*(\tau) = \exp(-\tau/t_*)$. t_* depends on the gridsize of the meteorological input data. It is the characteristic time it takes for a puff to reach the size of a grid-element. In the current version it is put 10^5 seconds (~30 hours), corresponding to a gridsize of approximately 60*60 km.

In the reservoir layer we set the constant c" to .4 $m^2 s^{-1}$ and in the mixed layer we used .6 $m^2 s^{-1}$, to fit the observations.

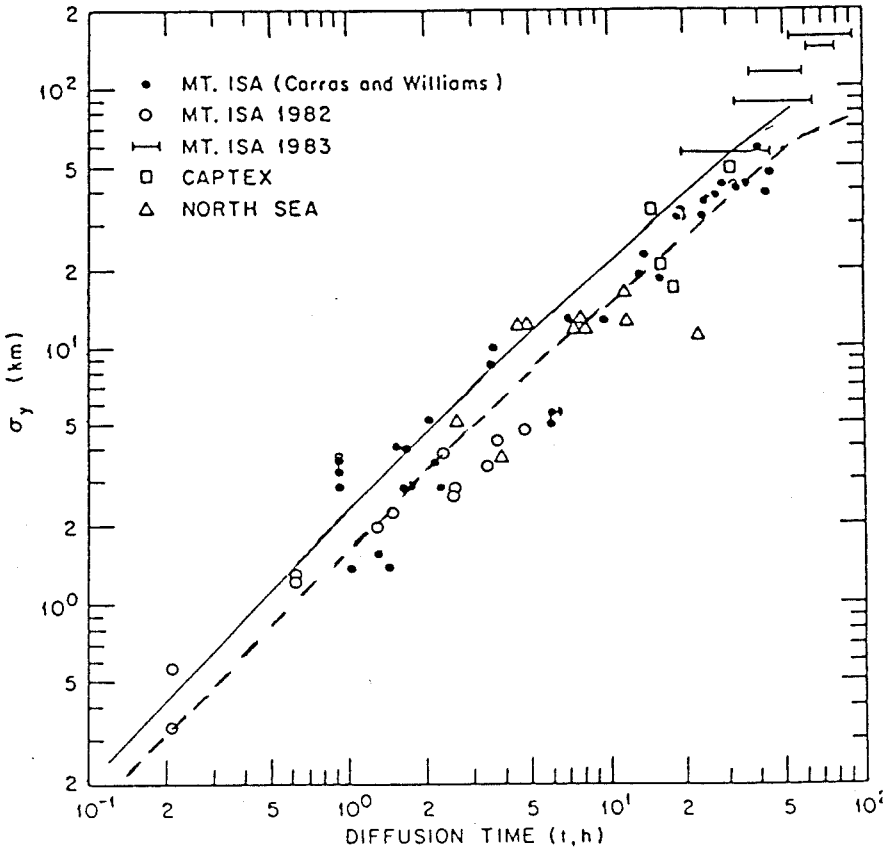

Figure 3 Composite of plume crosswind diffusion observations for mesoscale travel times compiled by Gifford (1985). Additionally, puff size as a function of time in the RIVM/KNMI Puff model is drawn: solid line for material in the mixed layer, the dashed line for material in the reservoir layer.

2.5 Vertical fluxes between both layers

During the journey of the puff, material may be transported from one layer to the other. In the model, the only way for material to cross the boundary between both layers is through variations of the mixing height.

The flux of material can be written as:

$$\text{Mass Flux} = w_e \cdot c(h) \qquad (13)$$

where c(h) is the concentration at the height z=h in the mixed layer or the reservation layer depending on the sign of w_e, and w_e is the entrainment velocity. At z=h, there is a discontinuity in the concentration profile. When w_e is positive the concentration in the reservoir layer ($c(z\downarrow h)$) is taken; when w_e is negative the concentration in the mixed layer ($c(z\uparrow h)$) is taken.

The entrainment velocity w_e is defined as:

$$w_e \equiv \frac{dh}{dt} - \overline{w}_h = \frac{\partial h}{\partial t} + \overline{u}_p\frac{\partial h}{\partial x} + \overline{v}_p\frac{\partial h}{\partial y} - \overline{w}_h \qquad (14)$$

$\overline{w}_h$ is the mean vertical velocity at z=h and $\overline{u}_p$ and $\overline{v}_p$ are the mean velocities in the x and y direction of the mass-centre of the puff.

In the model the vertical component of the wind $\overline{w}_h$ is neglected.

2.6 Advection of puffs

Wind analyses or prognoses on several grids are available to advect the puffs. To calculate the trajectory of the puff, the horizontal wind vector at the mass-centre of the puff is estimated by interpolation. Horizontally, this is done by simply taking the nearest gridpoint at which wind data are available. Vertically, interpolation or extrapolation of the available wind vectors at the nearest two levels takes place. Operationally, wind fields at only two or three heights are at our disposal (see section 3).

For vertical interpolation and extrapolation we use a power law for wind profiles. The power p can be obtained by:

$$p = \frac{\ln(\bar{u}(z_1)/\bar{u}(z_2))}{\ln(z_1/z_2)} \qquad (15)$$

where z_1 and z_2 are the nearest two heights for which the wind vectors are available. The wind speed at the mass-centre of the puff ($\bar{u}(z_p)$) is calculated by:

$$\bar{u}(z_p) = \left(\frac{z_p}{z_1}\right)^p \cdot \bar{u}(z_1) \qquad (16)$$

where z_p is the height of the mass-centre of the puff.

The direction of the wind at the mass-centre is also obtained by vertical interpolation using a weighting factor of $(z_p/z_1)^p$ similar to eq. (16).

The displacement $\vec{x}$ of the puffs is calculated by: $\vec{x} = \vec{u}(z_p).\Delta t$. To avoid large errors due to the discretization, the distance travelled by a puff in one timestep must be smaller than the grid-spacing of the input wind field. The timestep of the model is one hour; the grid spacing of the fine-mesh input data is ~60km (chapter 3).

2.7 Puff projection and puff splitting

-Puff projection-

Wind speed and wind direction are functions of space and time. A part of this variability is resolved by the wind fields that are used. The distinction between advection and turbulent diffusion is based on the resolution. Puff growth in subgrid scales is parameterized. The parameterization is described in sections 2.3 and 2.4. Dispersion on larger scales is resolved and dealt with explicitly by the model.

When the horizontal dimensions of the puffs reach the resolved scales (the grid spacings) of the wind field, the puffs are projected on the grid. For each grid cell, a new puff is generated that will be advected separately. The large projected puff is deleted (figure 4). When two or more puffs overlap, their contributions to the mass in a gridbox are added. The characteristics of the puffs, like layerheights, are weighted by mass for their contribution to the characteristics of the newly generated puff.

To put a restriction on the growth of the number of puffs, puff projection is performed only once a day.

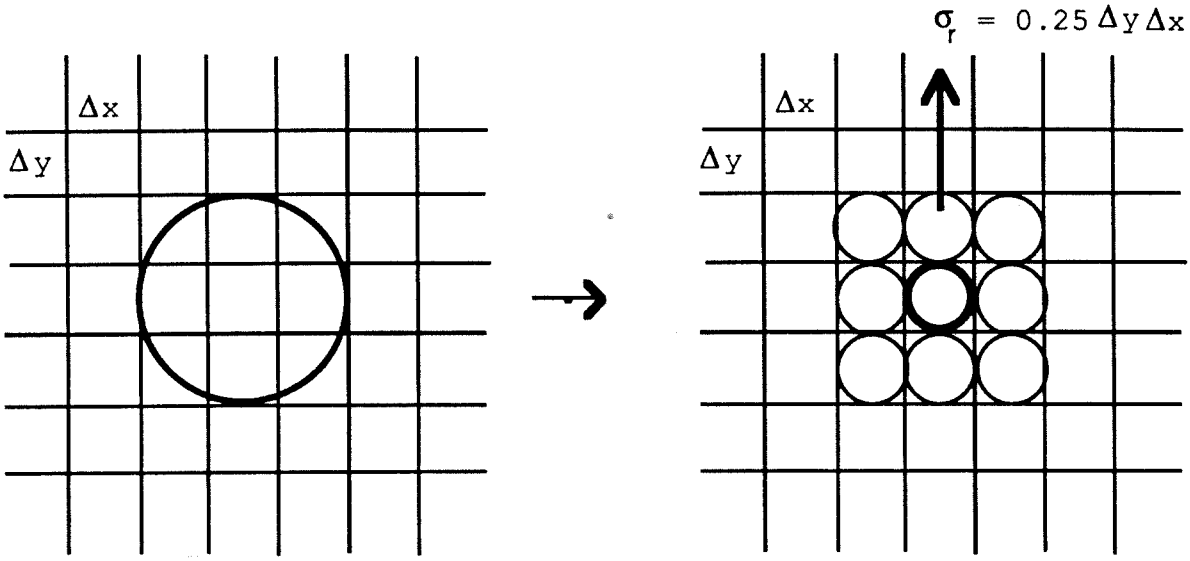

figure 4 Puff projection

-Puff splitting-
Horizontal wind vectors will also vary with height (vertical shear of the horizontal wind). The daily cycle of the height of the turbulent boundary layer, in combination with the daily cycle of wind shear, will cause material to disperse horizontally (e.g. McNider, 1988)
To account for this process, an algorithm is developed that splits a puff in two: a mixed layer puff and a reservoir layer puff. This will be the case over a land surface, at the end of the day, when stability changes sign and the nighttime boundary layer is formed. The two independent puffs will then be advected by a different wind vector (figure 5).
In general a puff will be split once a day, depending on the meteorological situation.

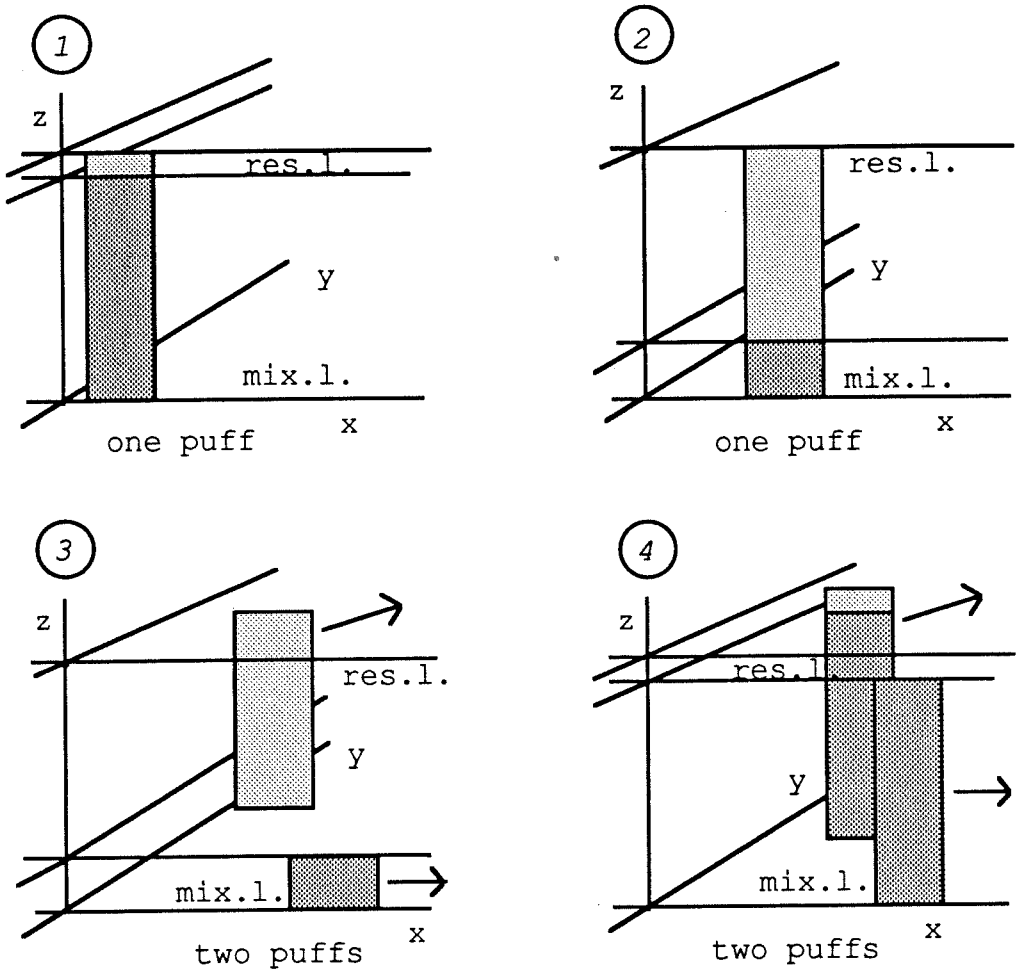

Stage *1*:One puff with mass in both layers;
Stage *2*:A shallow nighttime boundary layer is developed;
Stage *3*:The puff is split in two separate puffs, one in the mixed layer and one in the reservoir layer;
Stage *4*:A daytime mixed layer is developed; both puffs have mass in this layer.

Figure 5. Puff splitting depicted in 4 stages.

2.8 Dry deposition

Deposited material may contaminate the soil and field crops, and may contribute significantly to the human exposure to toxic substances or to radiation. Dry deposition and wet deposition are therefore important processes accounted for by the model

Dry deposition will reduce concentrations in the mixed layer. Material in the reservoir layer is decoupled from the surface and will therefore not be affected by dry deposition.

The dry deposition flux is calculated using the resistance model:

$$\text{Dry deposition flux} = V_g(z).c(z) = c(z)/(r_a+r_b+r_s) \quad , \quad (17)$$

where: $V_g(z)$ is the deposition velocity at height z ,
$c(z)$ is the concentration at height z,
r_a is the aerodynamic resistance,
r_b is the sublayer resistance and
r_s is the surface resistance.

-Surface resistance-
The surface resistance depends on characteristics of the dispersed material (like solubility and, for aerosols, the particle size), and on the characteristics of the surface. As an example, the surface resistance over a forest during nighttime for SO_2 and NO_x ($NO+NO_2$) is estimated between 700 and 2000 s/m. Over open water there is a large difference due to the different solubilities: r_c=0 s/m for SO_2 and approximately 700 s/m for NO_x (Voldner et al., 1986).

For most substances that may be released into the atmosphere the surface resistance can only be estimated crudely. In the model, r_c is a constant representing the whole model area and the dispersed material. The surface resistance needed for dispersion simulations following the Chernobyl disaster, were estimated to be ~500 s/m for both I-131 and Cs-137 (De Leeuw et al., 1986).

-Sublayer resistance-
The sublayer resistance r_b is defined as the resistance to transport from $z=z_0$ to z_{0c}, where z_0 is the roughness length for momentum and z_{0c} is the roughness length for transport of gases. It is parameterized by (Wesely and Hicks, 1977):

$$r_b = 2.6/(ku_*) \quad , \quad (18)$$

where u_* is the friction velocity, k is the Von Kármàn constant (k=0.4).

-Aerodynamic resistance-

The aerodynamic resistance r_a is the resistance to turbulent transport from a height z ($>z_0$) to the surface ($z=z_0$). It is assumed that pollutants and heat are transported in the same way, which implies that the exchange coefficient for heat can be used for gases as well. The resistance r_a is obtained by integration of $K_z(z)^{-1}$, the reciprocal exchange coefficient.

$$r_a = \int_{z_0}^{z} K_z(z)^{-1}\, dz = \int_{z_0}^{z} \frac{\phi_h(z/L)}{ku_* z} \qquad (19)$$

where $\phi_h(z/L)$ is the stability correction function for heat and L the Obukhov length. After carrying out the integration of (18) we get:

$$r_a = \frac{1}{ku_*} \cdot \{\ln(z/z_0) + \Phi_h(z_0/L) - \Phi_h(z/h)\} \qquad (20)$$

where Φ_h is the integrated stability correction function. For unstable situations (L<0) we used the formulation given by Dyer (1974) and Van Ulden and Holtslag (1985):

$$\Phi_h = 2\ln\left(\frac{1+y^2}{2}\right), \text{ where } y=(1-16z/L)^{-1/2} \qquad (21)$$

For stable situations (L>0) a formulation proposed by Holtslag and De Bruin (1988) is used:

$$-\Phi_h = a\frac{z}{L} + b\left(\frac{z}{L} - \frac{c}{d}\right)\exp\left(-d\frac{z}{L}\right) + \frac{bc}{d} \qquad (22)$$

where a=0.7, b=0.75, c=0.5 and d=0.35.

The derivation of the friction velocity and the Obukhov length from routine weather data is described in section 3.4.

2.9 Wet deposition

Wet deposition may bring large amounts of material down to the ground surface. The model can give valuable information to estimate human exposure. However, precipitation is on many occasions a subgrid process, therefore the model can only roughly estimate the wet deposition.

The below-cloud scavenging of polluted air by raindrops is parametrized as:

$$dc/dt = c \cdot \Lambda \quad , \qquad (23)$$

where c is the concentration of pollutant. The scavenging coefficient Λ depends on the spectrum of raindrop sizes, the solubility of the gas, the rain intensity and chemical properties of the pollutant and raindrop.

In the puff model we use the simple parametrization for the scavenging coefficient:

$$\Lambda = \zeta . I / d \quad , \qquad (24)$$

where I is the rain intensity and d the mixing height or the thickness of the reservoir layer. The scavenging ratio ζ is defined as:

$$\zeta \equiv c_{rain} / c_{air} \quad . \qquad (25)$$

The concentration in the raindrop (c_{rain}) is assumed to be in balance with the concentration in the surrounding air (c_{air}). It is assumed that scavenging takes place more efficiently in the reservoir layer than in the mixed layer, due to the difference of the drop spectra. The wash-out coefficient (ζ/d) is a uniform input parameter for each of the layers of the model, that is set according to the properties of the dispersed pollutant (e.g. $0.07 s^{-1} (m/h)^{-1}$ in the reservoir layer for I-131 and Cs-137 (De Leeuw et al., 1986)). The rain intensity I is drawn from the meteorological limited area model (FM-LAM, section 3.2)

In-cloud scavenging (or rain-out) is accounted for in a highly parameterized way by assuming a higher wash-out ratio in the reservoir layer.

2.10 Chemistry and radioactive decay

In the model radioactive decay and chemical reactions are sink terms. It is described by linear decay:

$$dc/dt = -K.c \quad , \qquad (26)$$

where K is the radioactive decay rate or chemical removal rate.

To estimate air concentrations at one position, contributions of a number of puffs are added. Chemical transformation, radioactive decay, dry and wet deposition are processes modelled in such way that they affect each separate puff. Consequently these processes can only be described by a linear expression like eq. (26). Chemical transformation or radioactive decay of material already deposited on the ground is not modelled.

3 Meteorological data

The model needs meteorological data to calculate advection, diffusion and deposition. Figure 6 depicts the flow and origin of meteorological data used by the dispersion model.

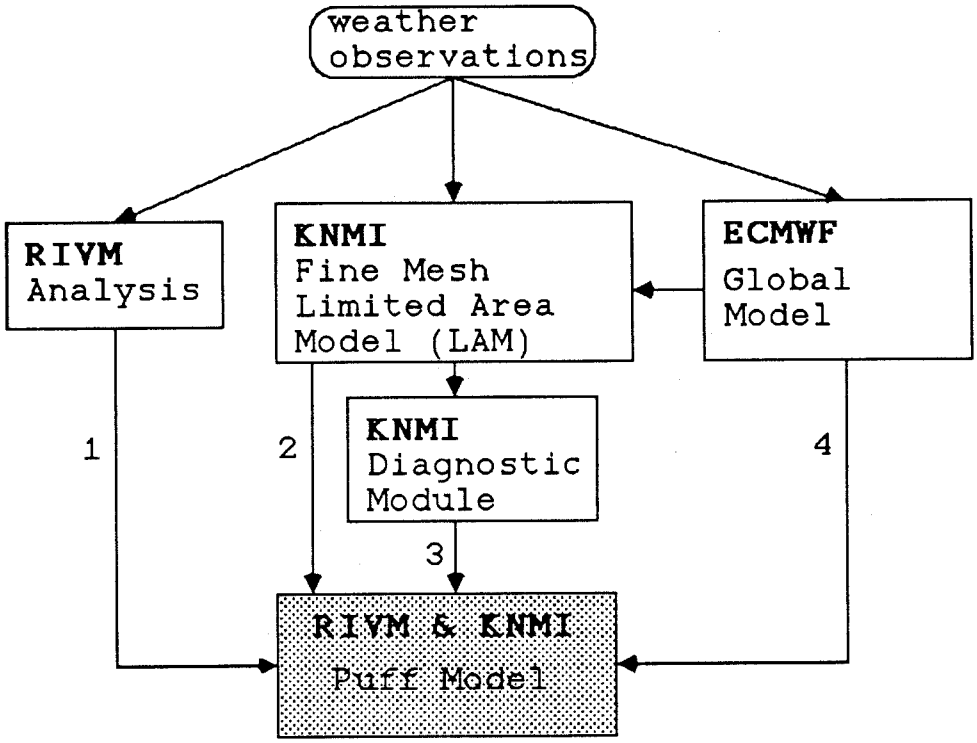

Figure 6 Flow and origin of meteorological information. (Numbers are explained in the text)

At RIVM hourly wind observations from the National Air Quality Monitoring Network (RIVM, 1990) are analysed for application in dispersion models covering The Netherlands and immediate surroundings (see figure 6,(1)). Prognostic computations for the European area need data from the ECMWF meteorological model (Louis, 1982), or the fine mesh version of this model: the KNMI FM-LAM (2 and 3). For calculations up to effectively 24 hours ahead, it is planned that the puff model uses the FM-LAM results. Results of the ECMWF model will then be used for computations effectively 24 hours up to 96 hours ahead (4).

At KNMI a postprocessor is developed (the Diagnostic Module) to derive the boundary layer height, the Obukhov length and the friction velocity from the FM-LAM (see par. 3.4)

Information about the meteorological input data is listed in table 2.

Table 2.
Description of the sources of meteorological information.

	SOURCES			
	ECMWF [1]	*KNMI FM-LAM* [2]	*KNMI DIAGNOSTIC MODULE* [2]	*RIVM ANALYSES* [3]
Meteorological Information	wind (p=1000mb, p=850mb)	rain wind (z~65m, z~500m, z~1500m)	h (u_*) [†] (1/L) [†]	wind (z=20m, z=150m)
Area	Europe (3000*3000km)	Europe (3000*3000km)	Europe (3000*3000km)	The Netherlands (400*400km)
Spatial Resolution	3°*3°	.55°*.55° (~60*60Km)	.55°*.55° (~60*60Km)	15*15Km
Time Resolution	6 Hours	3 Hours	3 Hours	1 Hour
Data Update Interval	24 Hours	3 Hours	3 Hours	1 Hour
Minimum Effective[‡] *Prediction Period*	72 Hours	24 Hours	24 Hours	-
References to fig. 6)	4	2	3	1

[†] *Used in future versions of the puff model, both at KNMI and RIVM*
[‡] *This means: the minimal length of the prediction period at any time*
[1] *Available at KNMI and RIVM*
[2] *Will come available to KNMI and RIVM during 1990*
[3] *RIVM only*

The choice of inputdata is based on three premises:
-1-small-scale data are of better quality than large-scale data;
-2-fields of analysed observations are better than prognostic fields generated by meteorological models;
-3-short prediction periods give better predictions than long prediction periods.

When all data described in table 2 are available, this leads to the sequence of input fields for one model run as depicted by figure 7.

Next sections describe wind (section 3.1), rain (section 3.2), mixing height (section 3.3) and L and u_* (section 3.4) in more detail.

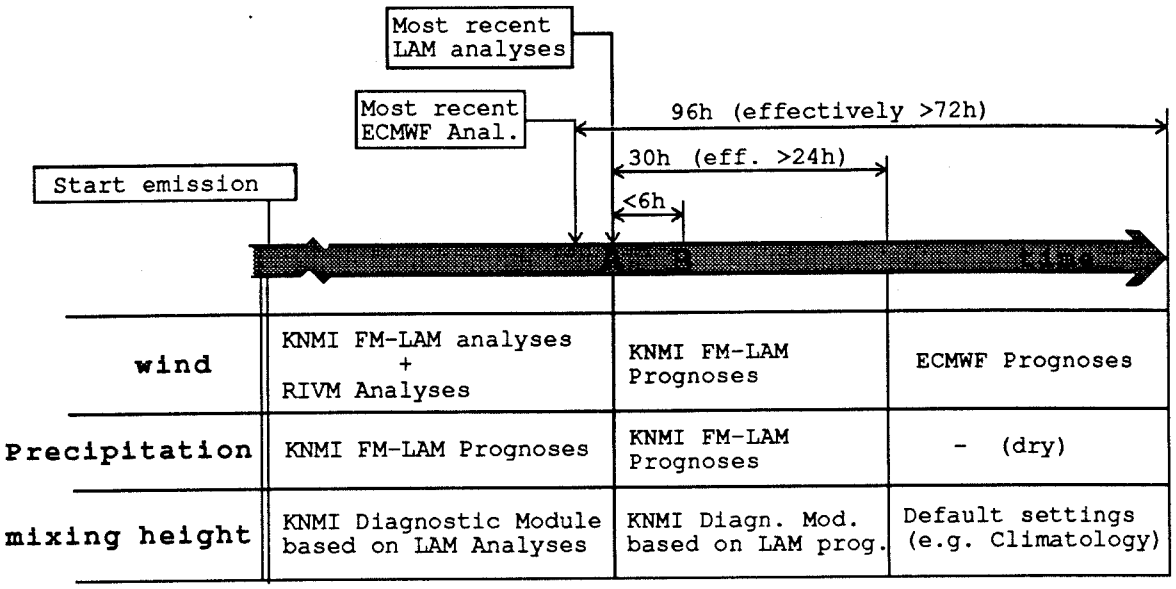

Figure 7. Data usage for one run of the RIVM/KNMI puff dispersion model. The real time (= the time at which the model is run) is somewhere on the time axis between A and B.

3.1 Wind

-RIVM wind analyses-

There are 33 meteorological stations included in the Air Quality Monitoring Network of The Netherlands (RIVM, 1990). The hourly wind speed and wind direction are on-line available at RIVM. Wind fields for The Netherlands and direct surroundings are obtained by spatial negative exponential interpolation of these observations. Wind fields at a higher altitude are obtained from the observations at the TV-towers (5 stations; 150-300m).

-ECMWF-

The EWCMWF model contains 19 layers with hybrid vertical coordinates (ECMWF, 1987). The lowest layers, that describe the planetary boundary layer, correspond to terrain-following sigma coordinates ($\sigma=P/P_{surface}$).

Physical parametrizations are applied on a Gaussian grid that corresponds to approximately 90km * 125km at a latitude of 55° north.

From this model horizontal wind velocities on two pressure levels are used for advection: p=1000mb and p=850mb, to which the heights z=200m and z=1500m are assigned. It is planned to use wind on model levels in the future. In the ECMWF model and the FM-LAM the difference between a terrain-following wind ($d\sigma/dt=0$) and horizontal wind ($dz/dt=0$) is small. This means that horizontal advection approximately follows the orography of

the meteorological model.

-KNMI FM-LAM-

The KNMI Limited Area Model is a fine-mesh version of the ECMWF global model used in short range weather forecasting. Grid spacing of this model is about 60*60km. Every 3 hours observations are assimilated and a calculation of the atmospheric situation 30 hours ahead is made. Horizontal wind velocities on 3 model levels (~65m, 500m and 1500m) are used for advection of puffs.

3.2 Precipitation

To estimate wet deposition the rain intensity I is needed (eq. 24). Frontal activities may cause precipitation from stratiform clouds in a large area that may be resolved by the FM-LAM. Convective precipitation takes place on subgrid scale and can only be handled in a statistical way by the meteorological models.

The ECMWF model and the FM-LAM do not make an analyses of observed precipitation. The models do however produce precipitation, and distinguish between convective precipitation, frontal precipitation and other kinds of precipitation (snow/hail/rain). It is planned to use total precipitation from the FM-LAM, accumulated over 3 hours (R) and to assume it to be rain. The average intensity for one grid element is calculated by taking $I=R/3$ (mh^{-1}), where R is the cumulative precipitation amount.

For calculations more that 30 hours ahead, the combination of a coarse grid and the large prediction period make the precipitation data derived from the ECMWF model less reliable than the FM-LAM data. It is therefore decided not to use ECMWF precipitation data, and to omit wet deposition during this period (see figure 4).

3.3 Mixing height

When the KNMI FM-LAM comes available, the mixing height used in the model will be a function of position. The mixing height from the start of the emission until approximately 24 hours ahead, is obtained from the Diagnostic Module (DM). (For a detailed description of the methods used in the Diagnostic Module is referred to Holtslag and Van Westrhenen (1989).)

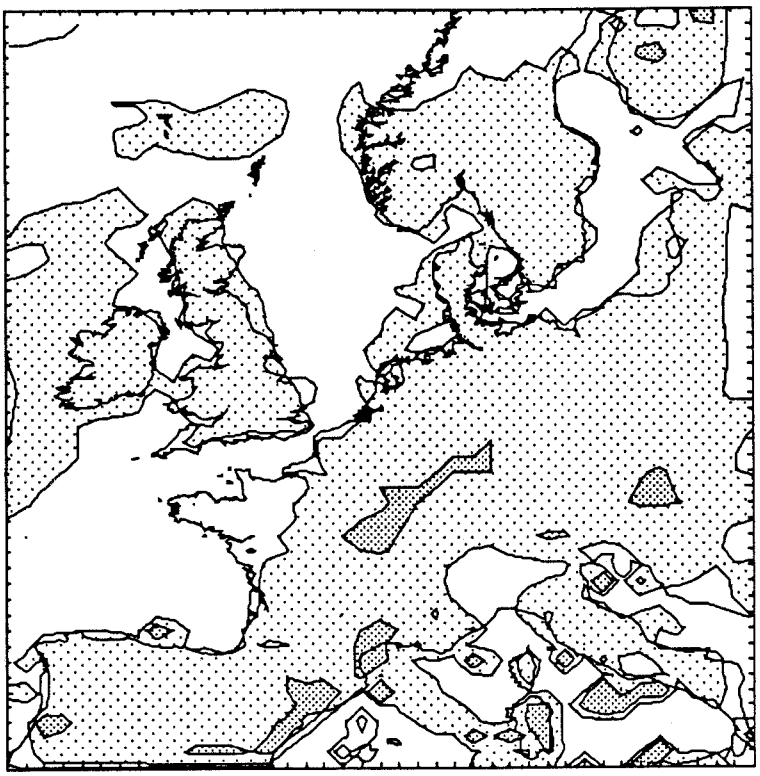

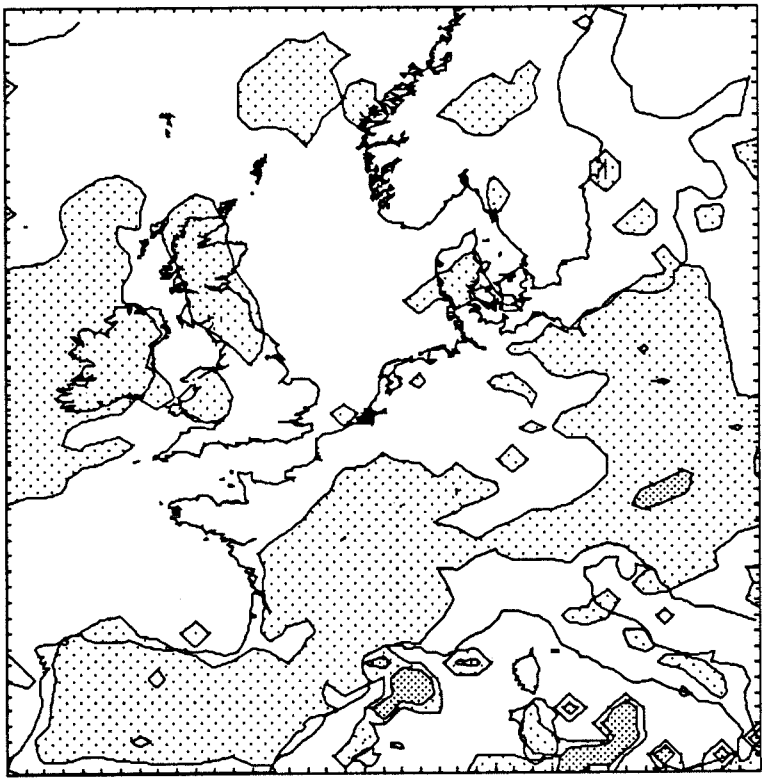

Figure 8 Examples of mixing heights during daytime (**A**) and in the evening (**B**) based on FM-LAM.
Grey areas: h>500m; dark grey areas: h>1000m.

In stable situations (L>0) a formula derived by Nieuwstadt (1981) is used:

$$h=\frac{c_1 u_*/f}{1+\frac{c_1}{c_2}h/L} \qquad (27)$$

where $c_1=0.15$ and $c_2=0.70$.

In unstable situations (L<0) the dry parcel intersection method[3] conform Troen and Mahrt (1986) is used to estimate the height of the convective boundary layer. Figure 8 shows examples of the mixing height during daytime (fig. 8A) and during nighttime (fig. 8B).

The Obukhov length and the friction velocity needed in equation (27) are derived by the Diagnostic Module, on the basis of KNMI-LAM outputs. These quantities are not used in the puff model itself. In the present version of the model we use a uniform u_* and L, that are only a functions of time. The scheme used for their derivation is explained in the next section.

When calculations are made more than 30 hours ahead, the ECMWF model is the only source of meteorological information. For this period we assume a uniform field of mixing heights for the whole model area. Climatological values may be used for the maximum mixing height. Linear growth is assumed during daytime. This results in pictures like figure 9, showing the (uniform) mixing height as a function of time.

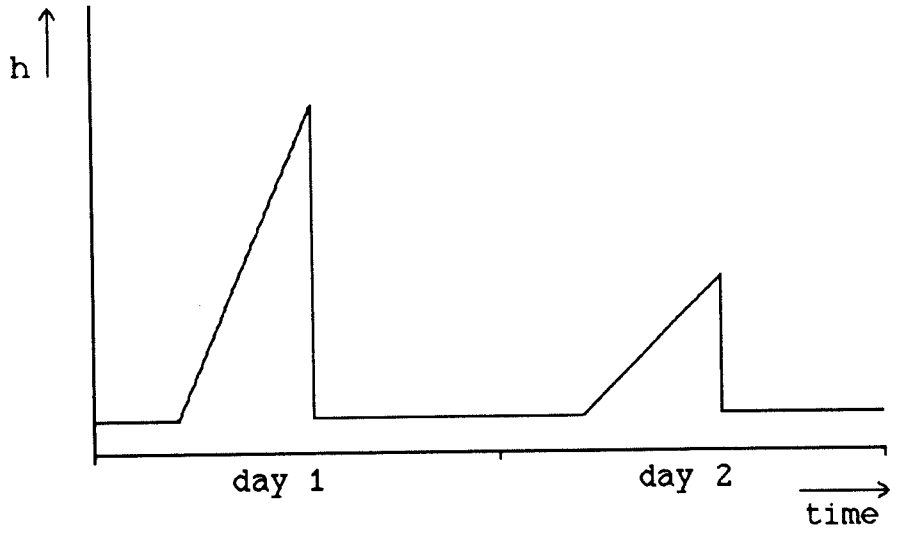

Figure 9 An example of the diurnal cycle of uniform mixing height.

[3]A parcel is lifted from near the surface to the height of the convective boundary layer h_c. This height is reached when the virtual potential temperature of the parcel is equal to the virtual potential temperature of its environment.

3.4 Obukhov length and friction velocity

The Obukhov length (L) and the friction velocity (u_*), are needed to estimate the dry deposition flux and vertical dispersion. In the current model a rough estimate of u_* and L is made, uniform over the whole model area. Future versions of the model will use input fields of u_* and L from the Diagnostic Module.

To calculate the friction velocity and the Obukhov length over a land surface, schemes from Van Ulden and Holtslag (1985) and Holtslag and De Bruin (1988) are followed. An iteration procedure between equation (28) and (29) yields u_* and L:

$$u_* = k.\bar{u}(z).[\ln(z/z_0) - \Phi_m(z/L) + \Phi_m(z_0/L)]^{-1} \qquad (28)$$

where :

$$\Phi_m = 2\ln\left(\frac{1+x}{2}\right) + \ln\left(\frac{1+x^2}{2}\right) - 2\tan^{-1}(x) + \frac{\pi}{2},$$

$$\text{where } x = \left(1-16\frac{z}{L}\right)^{-\frac{1}{4}}, \qquad \text{for } (z/L) < 0;$$

$$\Phi_m = -a.\frac{z}{L} - b.\left(\frac{z}{L} - \frac{c}{d}\right).\exp\left(-d\frac{z}{L}\right) - \frac{bc}{d}, \qquad \text{for } 0<(z/L)\leq 200;$$

$$\Phi_m = -a.\frac{z}{L} - \frac{bc}{d}, \qquad \text{for } (z/L) > 200 ;$$

(a=.7, b=.75, c=5, d=.35)

$$\text{and} \quad L = -\frac{\rho C_p T u_*^3}{kgH} . \qquad (29)$$

The wind speed $\bar{u}(z)$ is the average wind speed of the lowest wind field. The sensible heat flux (H) is estimated by a model of the surface energy balance using solar elevation. Cloud-cover, the soil moisture parameter (α), temperature (T) and the roughness length (z_0) are input to the model. For each of these parameters

a value representing the whole model area is chosen, and updated once a day.

4 Application to the Chernobyl accident

The RIVM/KNMI puff model has been applied to the Chernobyl accident. Emissions from the reactor approximately started at 26th of April 1 UTC. The dispersion of I-131 and Cs-137 has been simulated for nearly nine days. For most parts of Europe radioactivity measurements during this period were available for comparison with model values.

4.1 Short description of the meteorological situation

At the time the emission started a high pressure system dominated north-west Russia (figure 10A). The first two days of the emission, material was transported to Scandinavia. Weak frontal systems extending from Scandinavia southward towards Italy were present. Rainfall occurred around the Baltic sea, bringing down debris from the reactor. A high pressure system moved from Bretagne over The Netherlands to Denmark (figure 10B), causing transport of material south-westwards to Central Europe (30/4 to 2/5). A high pressure area developed over the Baltic Sea (figure 10C), and material moved to the north west, partly over The Netherlands and Great Britain (2/5 to 4/5).
A detailed description of the meteorological situation during the Chernobyl episode is given by Smith and Clark (1989).

4.2 Specification of the source term, parameter settings and meteorological data used

-Source term-
In this case-study the source term and parameter settings used are the same as defined in the model intercomparisson study ATMES[4]. Figure 11 A and B gives the daily emission of Cesium 137 and Iodine 131 respectively. The effective emission height is also indicated.

-Parameter settings-
The half life of I-131 due to radioactive decay is put 8.05 days. Radioactive decay of Cs-137 is neglected.

Wash-out coefficients are chosen: .0111 $s^{-1}(m/h)^{-1}$ for the mixed layer and .070 $s^{-1}(m/h)^{-1}$ for the reservoir layer. In the calculation of the deposition a surface resistance of 500 s m^{-1} is assumed.

[4]The Atmospheric Transport Model Evaluation Study (ATMES) is initiated by the WMO, IAEA and CEC. Results of ths study are expected in spring 1991.

-Meteorological data-
The meteorological fields used for this exercise are not the same as what will be used in a real-time situation as described in the previous chapter. For this case-study, calculations are made using KNMI FM-LAM precipitation and wind data. The wind fields are observation analyses produced by the analyses system of the KNMI FM-LAM. The 1000mb and 850mb wind fields are used. The heights to which the wind vectors are assigned are 200m and 1500m. Every 3 hours a new set of input data is used. Linear interpolation in time is performed for the intermediate hours.

The accumulated precipitation is a 3 hour forecast, since the meteorological model cannot provide analysed precipitation data. The precipitation amounts are divided equally over three hours.

The mixing heights for this study are obtained from schemes developed by various authors, using observed temperature profiles, sea water temperatures and cloud cover observations (Verver and Scheele, 1988).

4.3 Results and discussion

Nine days of the dispersion of Cs-137 have been simulated (the total simulation time was 222 hours). Figures 12A to 12D show the distribution of air concentrations of Cs-137 near the surface (z~4m). Figure 13 shows the total accumulated wet and dry deposition of Cs-137, up to the 5th of May, 6 UTC.. On the edges of the figure the grid spacings of the model are indicated.

During the first few days material is transported towards Sweden. In a second stage a flow to the south-west moves material into Central Europe. Air concentrations decreased, due to radioactive decay, precipitation and dry deposition.

In figures 12B and 12C it is shown how material covers large parts of Europe during the next days. Figures 13B and 13C reveal high deposition areas in the south of Germany and a part of northern Italy.

On the 4th of May, material moved further to the north-west (figure 12D).

-Comparison of model values with observations-
Table 3 gives the total accumulated dry and wet deposition of Cs-137 up to 5/5/1986, 6 GMT for most European countries. For comparison etimates of the total deposition based on observations in some European countries are also given. There is a good agreement between the observations and the model values. However, a substantial amount of Cs-137 was still in the atmosphere on May 5th, contributing to the observed depositions, but not simulated by the model.

Figure 14 shows the locations where measurements of air concentrations of I-131 are available. The observational data of I-131 presented are taken from De Leeuw et al. (1986). Figure 15A depicts model concentrations and observed concentrations versus time.

The first days after the initial release material was transported directly to Scandinavia. Its arrival in Stockholm was modeled approximately 6 hours too soon. Concentrations are overestimated by a factor ~2. One and a half day later, concentrations began to rise in Budapest, which was also found by the model. The first peak concentration (April 30) found by the model coincides with the high concentrations that were observed. High concentrations found on the first of May are not simulated well.

Model concentrations for Vienna compared very well with observations (observations were only available from 108 to 142 hours after the initial release).

The arrival time in Garmisch Partenkirchen (FRG) is estimated well, but the maximum concentration on the first of May is underestimated by a factor ~5.

In Paris and Bilthoven the time of the model concentration maximum nearly coincides with the maximum observed. The concentrations themselves are underestimated (Paris a factor of ~10, Bilthoven by a factor ~3)

Peak values found in Braunschweig (FRG) is simulated fairly well, although concentrations are overestimated by a factor of 2 to 3. The peak value on the 4th of May is overestimated.

Model concentrations for Varese in Italy are simulated well up to the first of May. On May 2 and 3, model values deviate severely from what is observed. One reason (among many others) could be the location of this site near the Alps. The representation of mountains by the KNMI-LAM is rather coarse, the local wind is therefore not be represented accurately

The results for Marcoule in the South of France show a similar kind of deviation as in Varese.

The timing of the high concentrations in Harwell (UK) is reproduced fairly well, concentrations are underestimated by a factor ~3.

The ability to predict arrival time is a useful feature of the model. The accuracy of the concentration estimates is much lower. There are several uncertain factors influencing the observed concentration data, such as:

-the source characteristics,
-subgrid phenomena (orography, coastlines, precipitation, clouds),
-measurement accuracy.

Large concentration gradients in the plume (occurring during the first few days), makes model results very sensitive to the advection speed and direction.

Keeping the factors mentioned above in mind, it is concluded that the model gives reasonably good estimates for the air concentrations and that it gives good estimates of the arrival times.

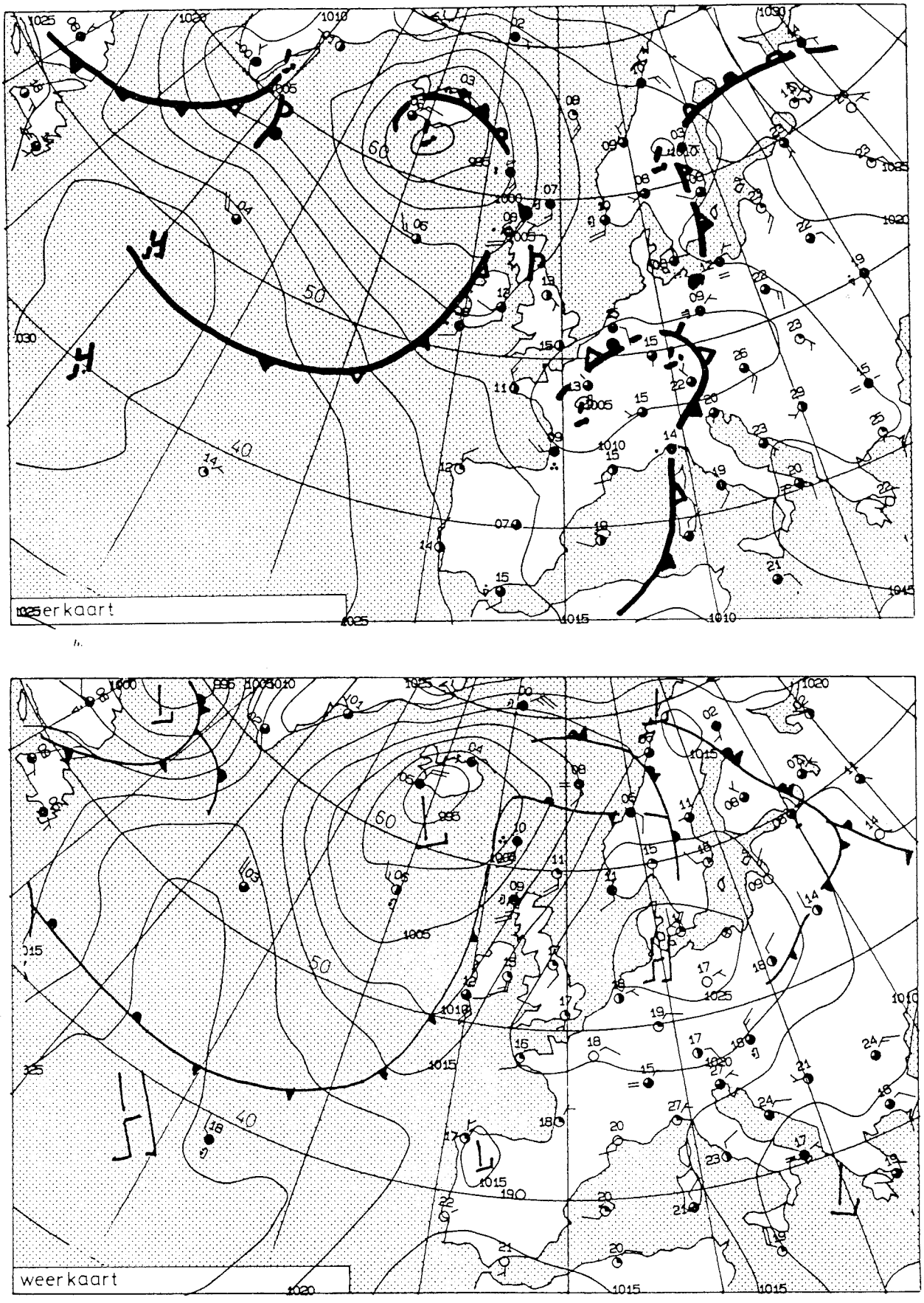

Figure 10 A and 10B Surface weather maps for April 26 1986 12 UTC (upper), and May 1 1986 12 UTC.

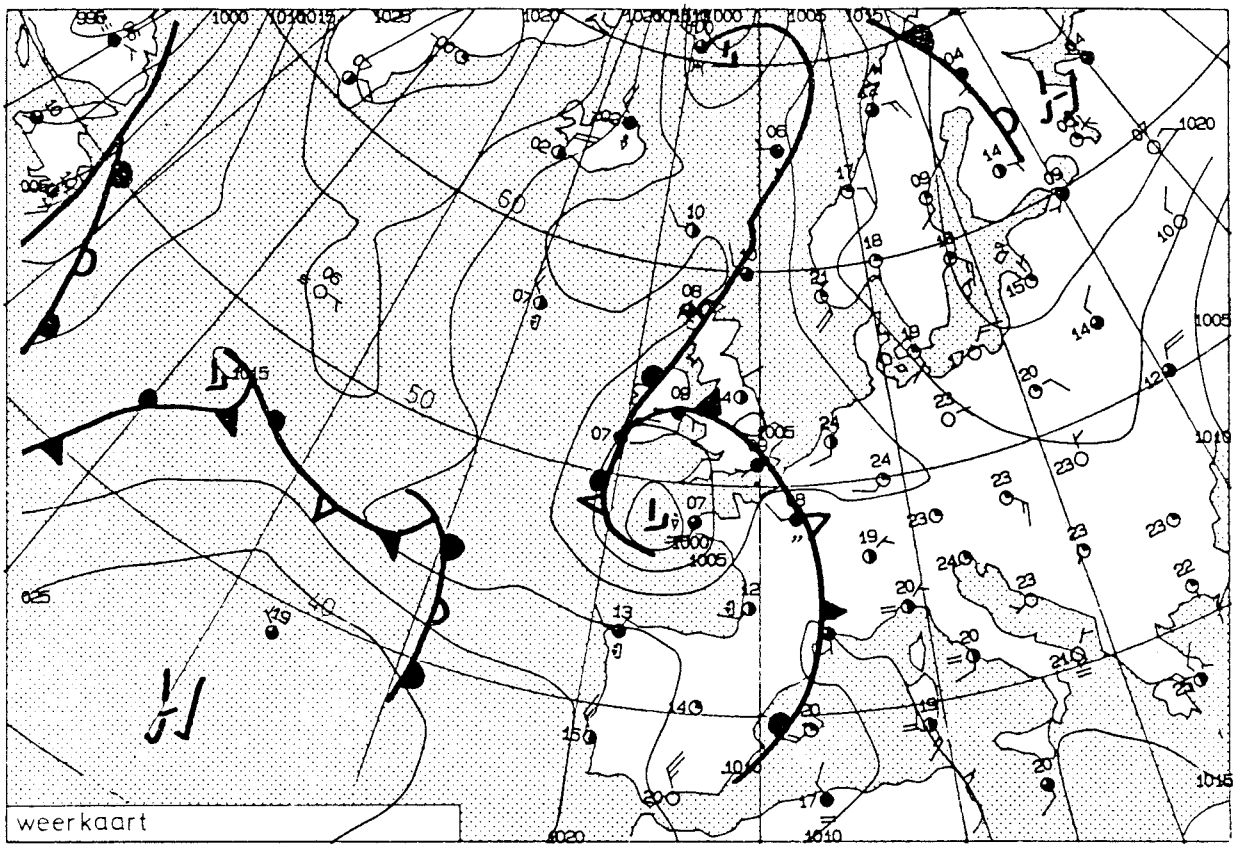

Figure 10 C Surface weather map for May 3 1986 12 UTC.

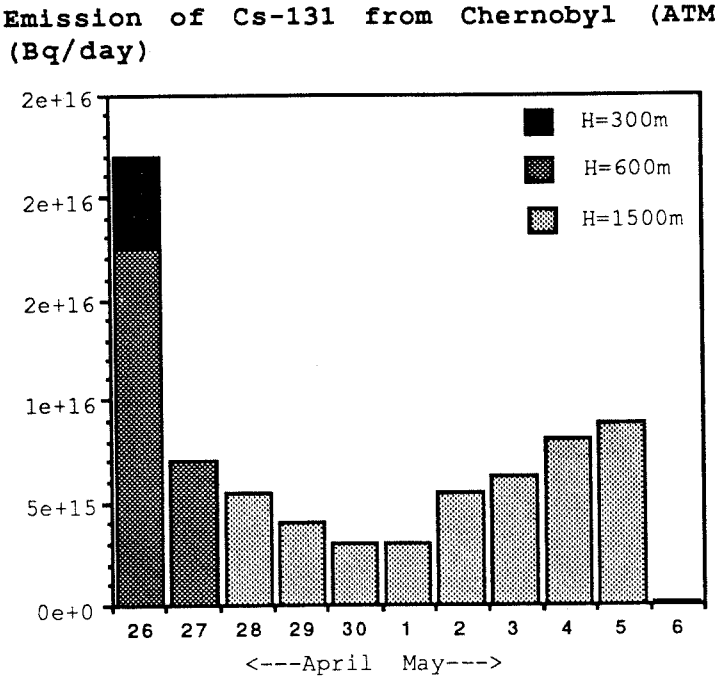

A

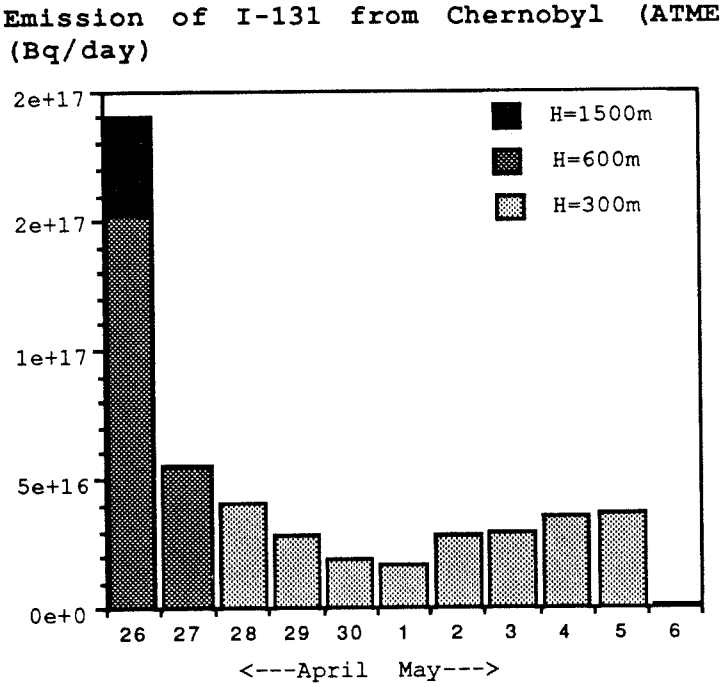

B

Figure 11 Emission data used in the model intercomparison study ATMES. Depicted are the emission height H and the emitted amount of Cs-137 (**A**) and I-131 (**B**) for each day.

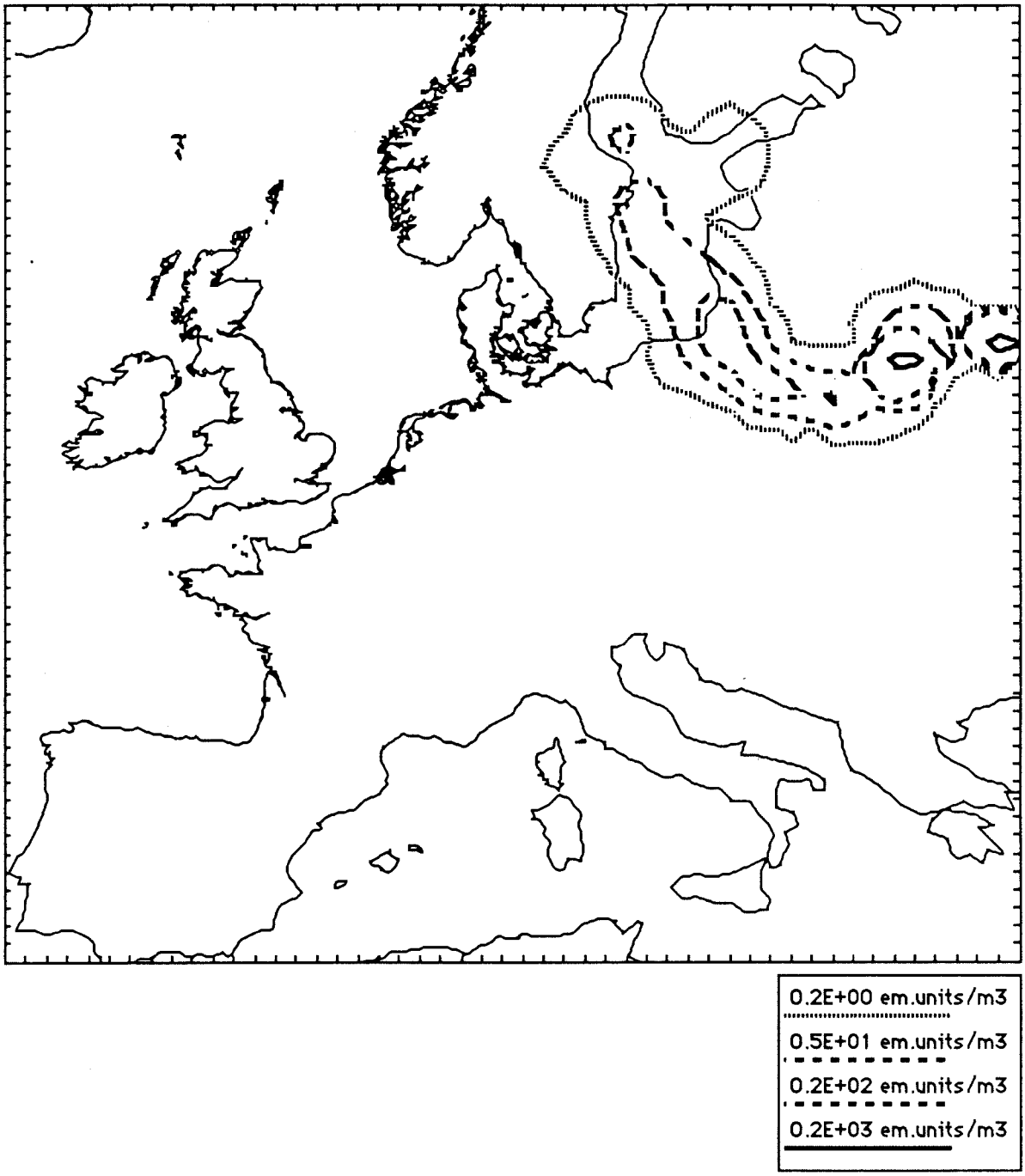

Figure 12A. Concentration distribution of Cs-137 over Europe for April 28 1986, 12 UTC. KNMI/RIVM Puffmodel.

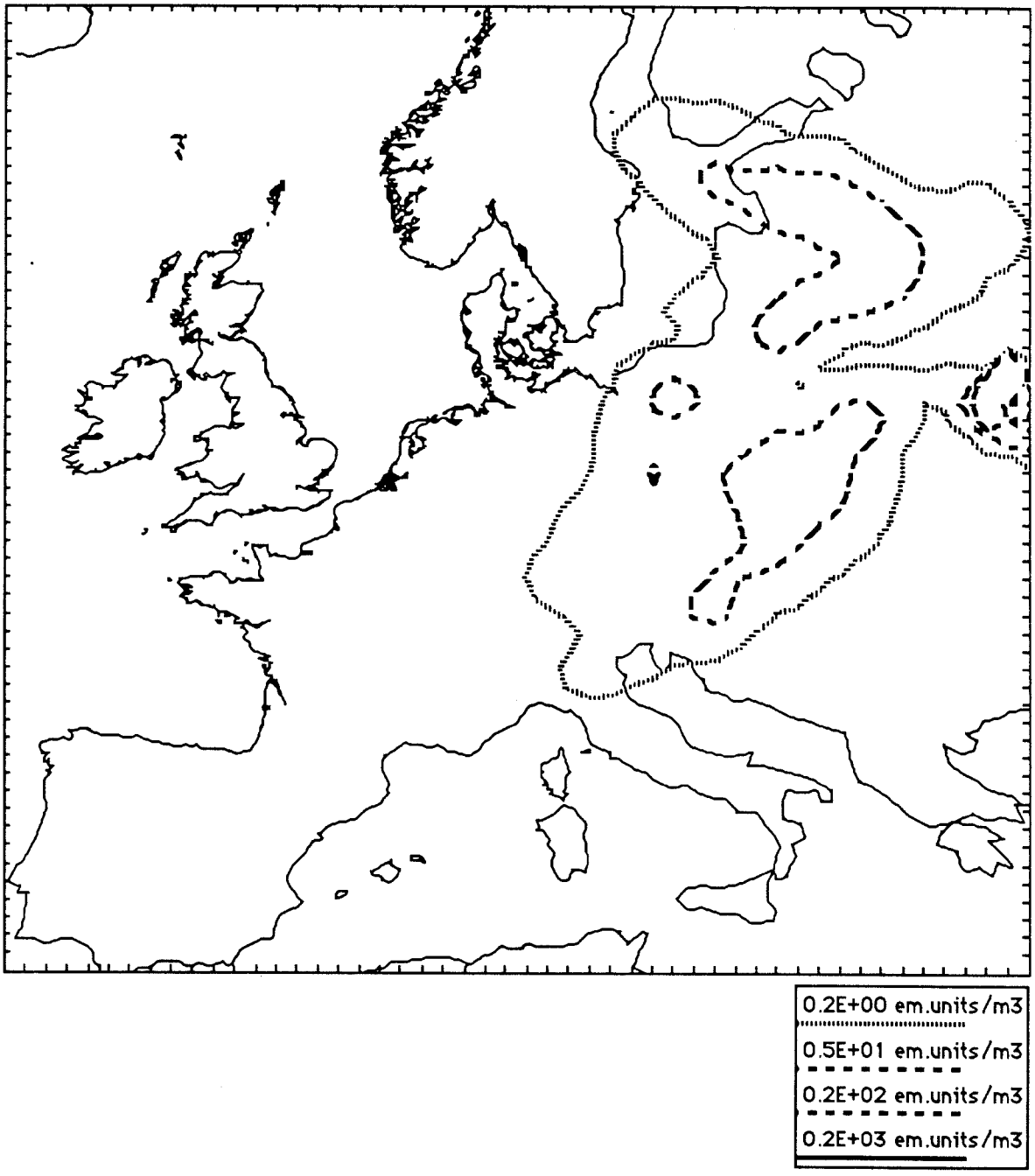

Figure 12B. Concentration distribution of Cs-137 over Europe for April 30 1986, 12 UTC. KNMI/RIVM Puffmodel.

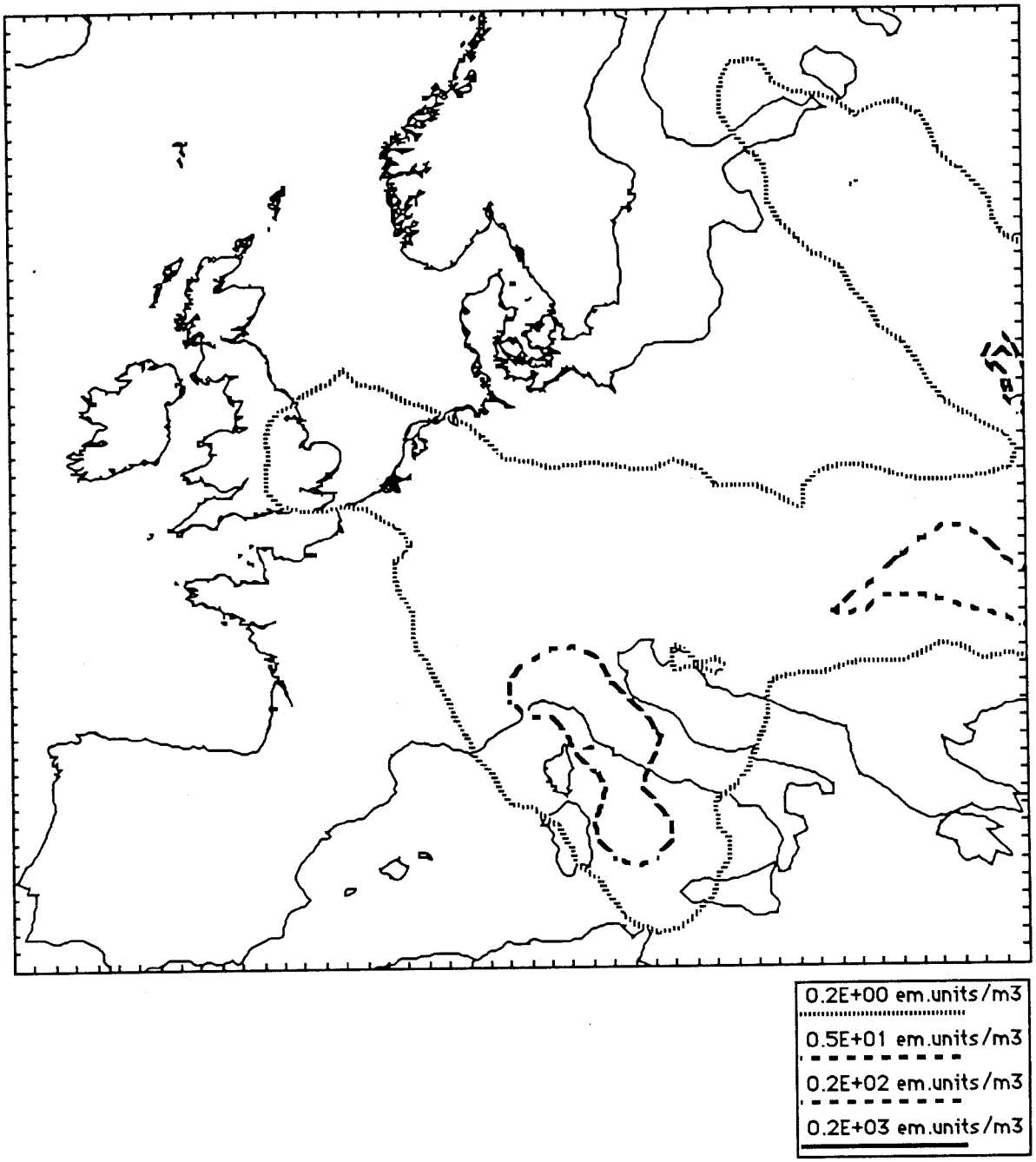

Figure 12C. Concentration distribution of Cs-137 over Europe for May 2 1986, 12 UTC. KNMI/RIVM Puffmodel.

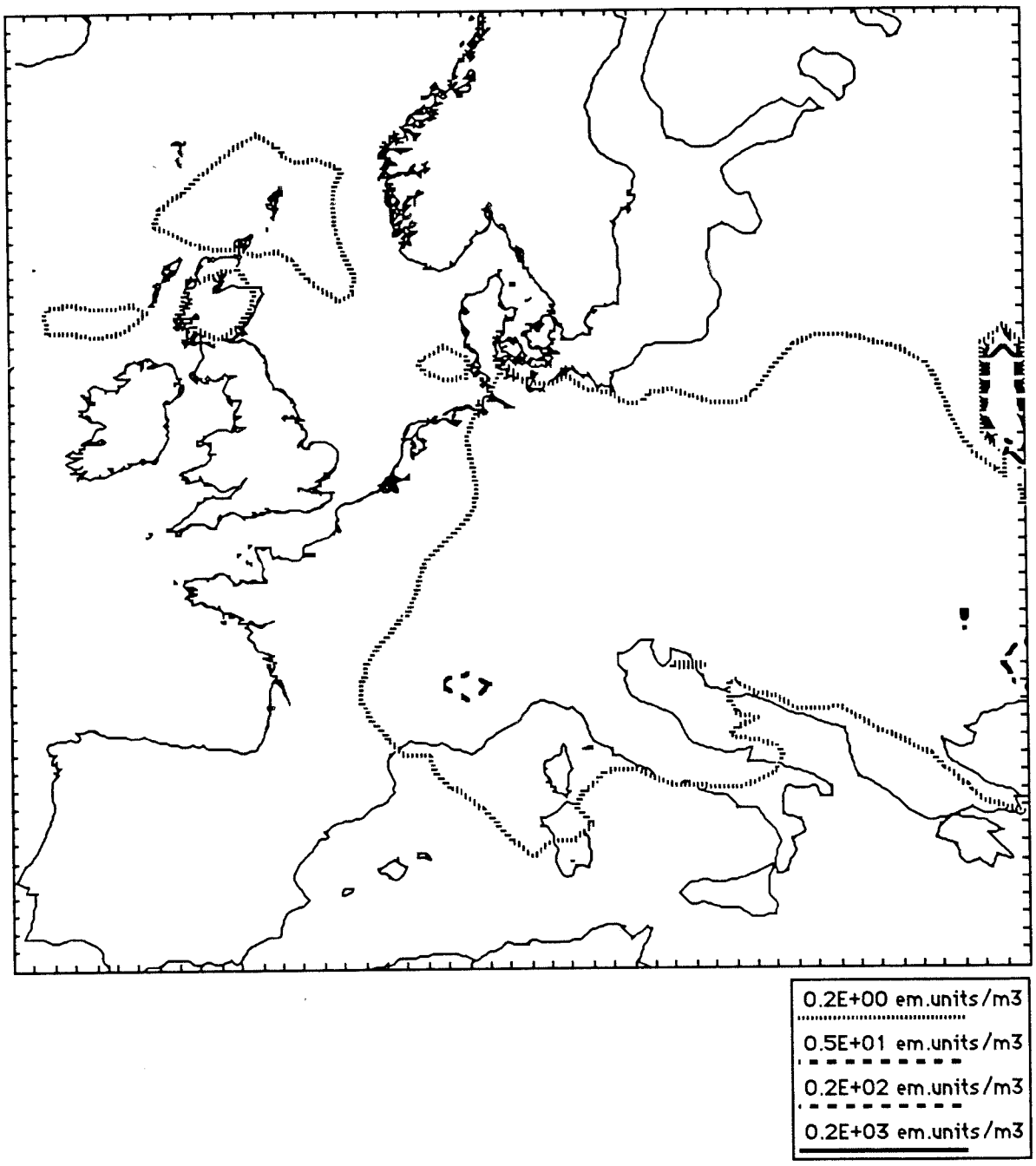

Figure 12D. Concentration distribution of Cs-137 over Europe for May 4 1986, 12 UTC. KNMI/RIVM Puffmodel.

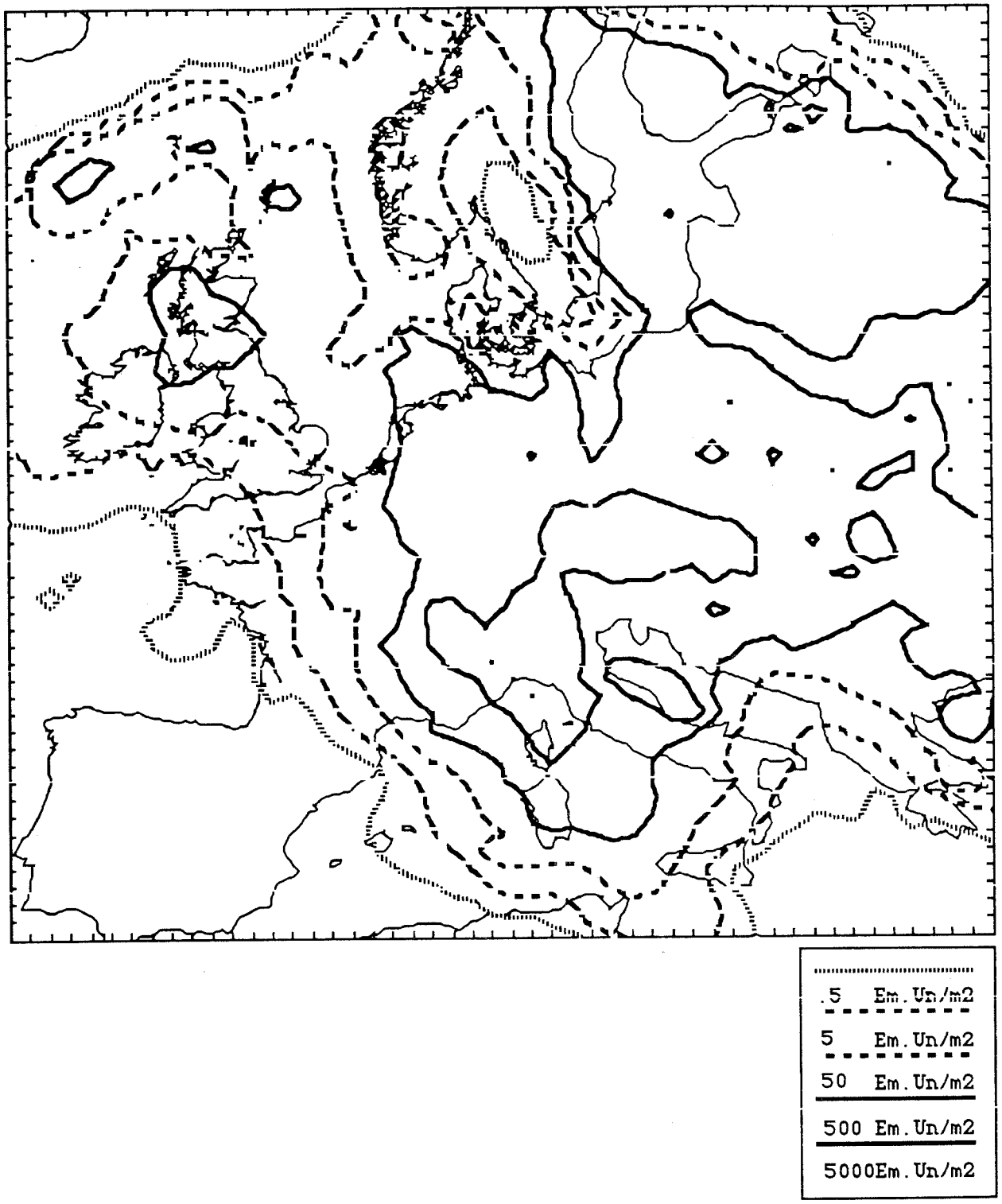

Figure 13. Accumulated (dry and wet) deposition of Cs-137 over Europe up to May 5, 6 UTC. KNMI/RIVM Puffmodel.

Table 3 Total accumulated dry and wet deposition of Cs-137, up to 5/5/1986 6 GMT (for the model values), for some countries. Observations refer to the whole period (OECD,1987; CCRX,1988).

COUNTRY	No.GRIDPOINTS	MODEL	OBSERVATIONS
ALBANIA	6	.0	
BELGIUM	7	1.9	.8
W.-GERMANY	63	4.6	4.0
BULGARIA	16	1.9	
E.-GERMANY	29	.6	
DENMARK	8	.1	.8
FINLAND	43	.7	
FRANCE	144	1.9	1.3
GREECE	29	.3	3.5
GREAT-BRITAIN	56	.3	.9
HUNGARY	22	4.2	
IRELAND	17	.1	
ITALY	73	4.9	6.0
YUGOSLAVIA	74	1.2	
NETHERLANDS	11	1.4	1.8
NORWAY	53	.0	
AUSTRIA	24	8.7	15.0
POLAND	73	2.9	
PORTUGAL	23	0.0	
ROMANIA	58	3.4	
SOVIET-UNION	315	4.9	
SPAIN	131	0.0	.0
CZECHOSLOVAKIA	39	6.2	4.0
ICELAND	11	0.0	
SWEDEN	86	4.7	8.0
SWITZERLAND	12	8.8	7.1
NORTHERN AFRICA	20	0.0	
NORTH SEA	222	.2	
ATL. OCEAN NORTH	369	.1	
ATL. OCEAN SOUTH	176	0.0	
MEDITERRANEAN	418	.6	
BALTIC SEA	117	8.5	

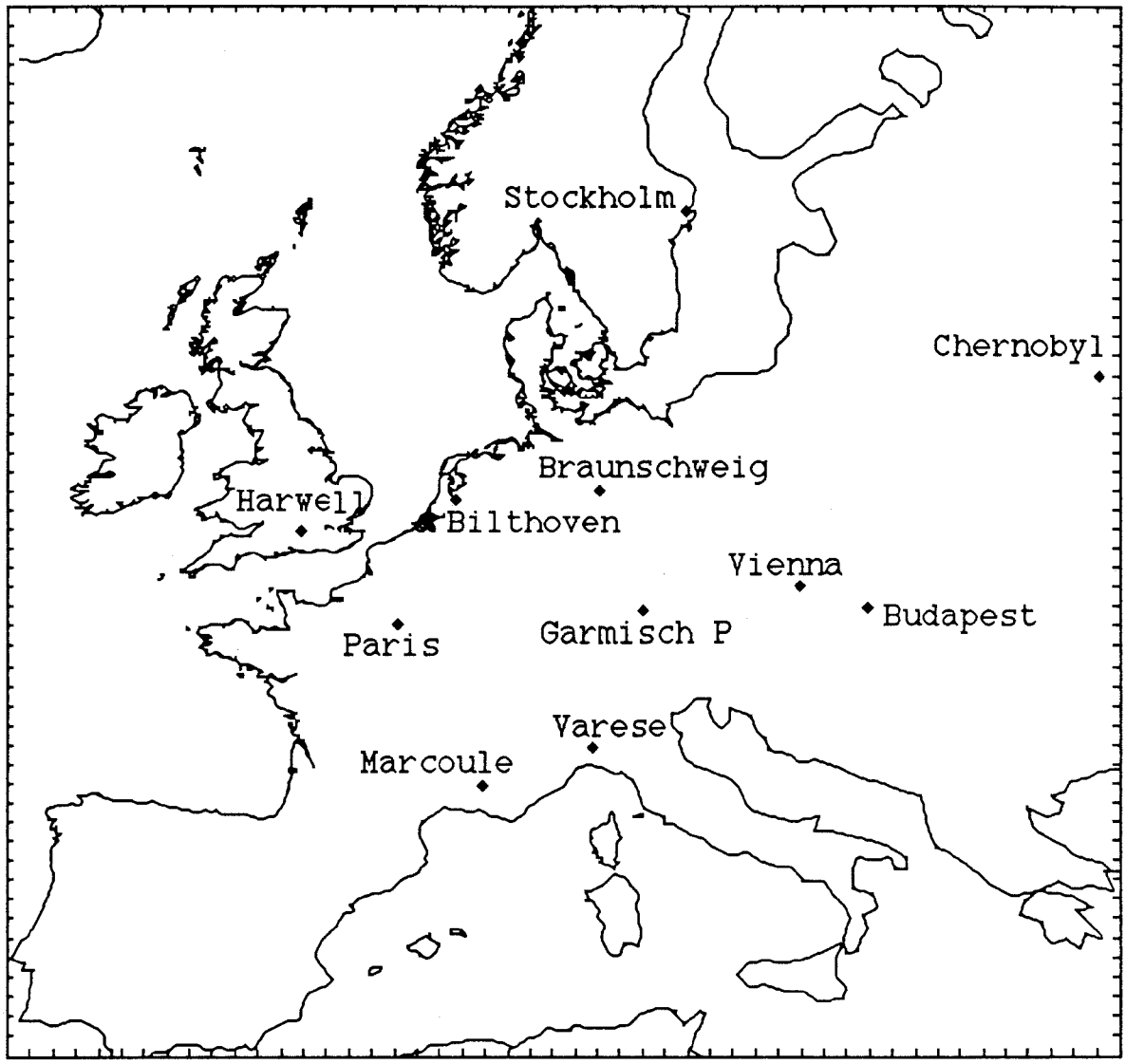

Figure 14.Locations where air concentrations of I-131 are measured. These data are compared with model output.

Figure 15 Model concentration and observed concentrations of I-131 for 10 European sites.

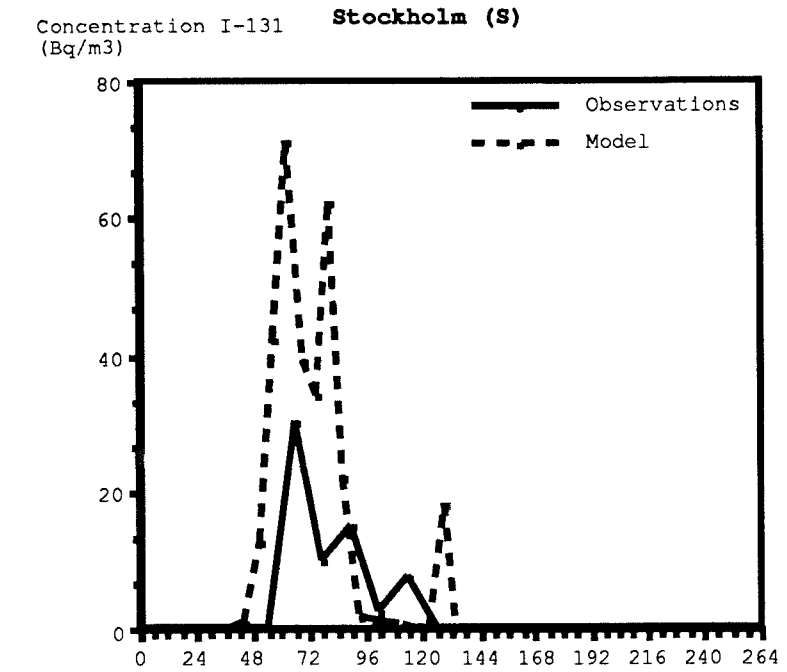

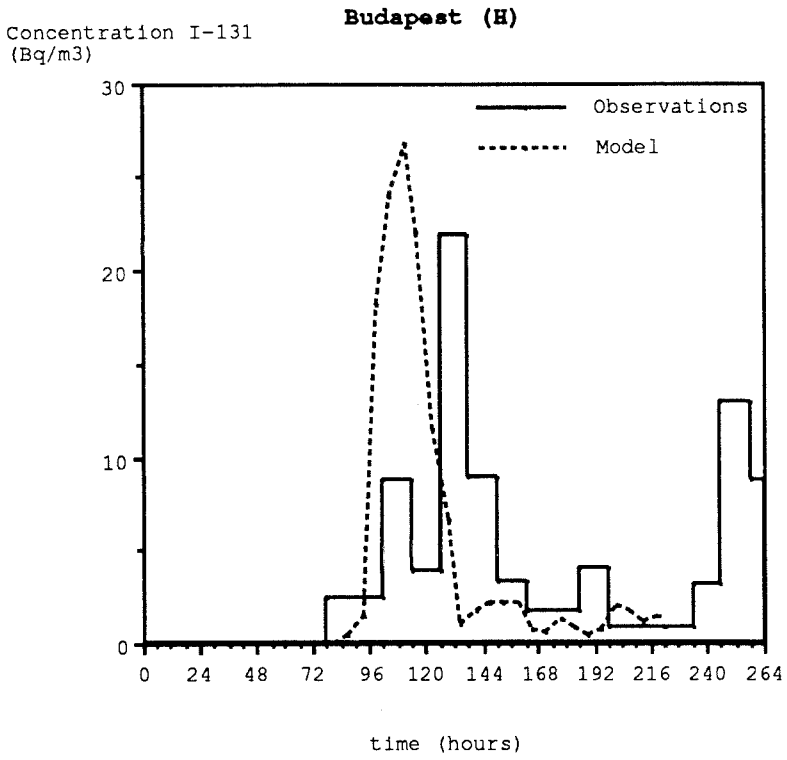

Vienna

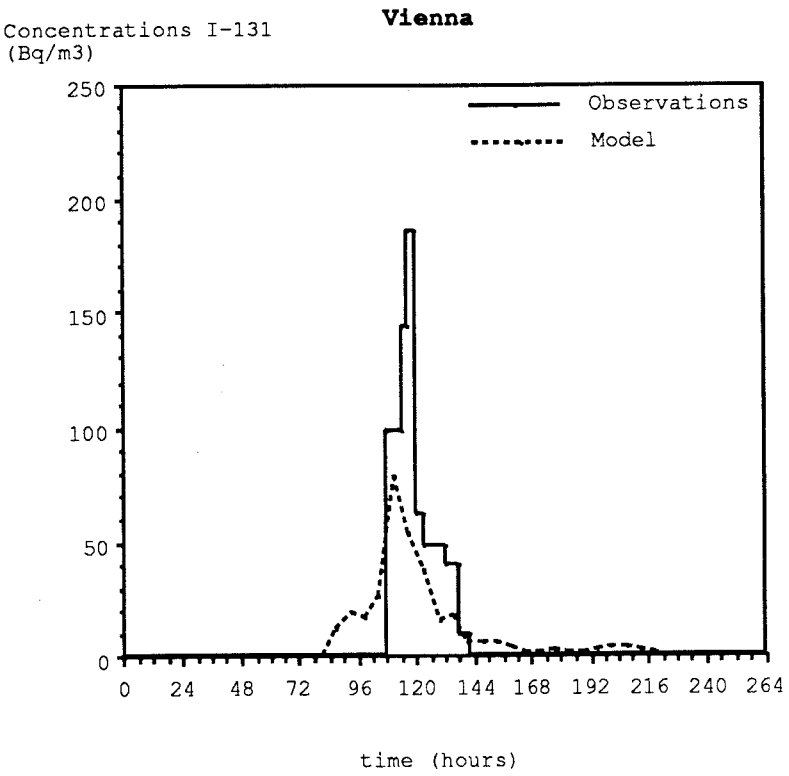

Garmisch Partenkirchen (FRG)

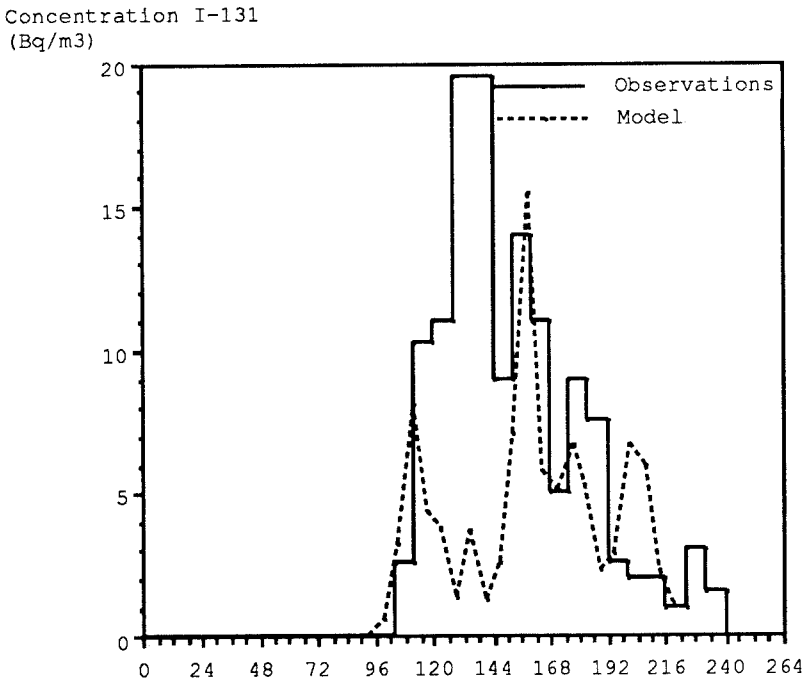

Paris

Concentrations I-131
(Bq/m3)

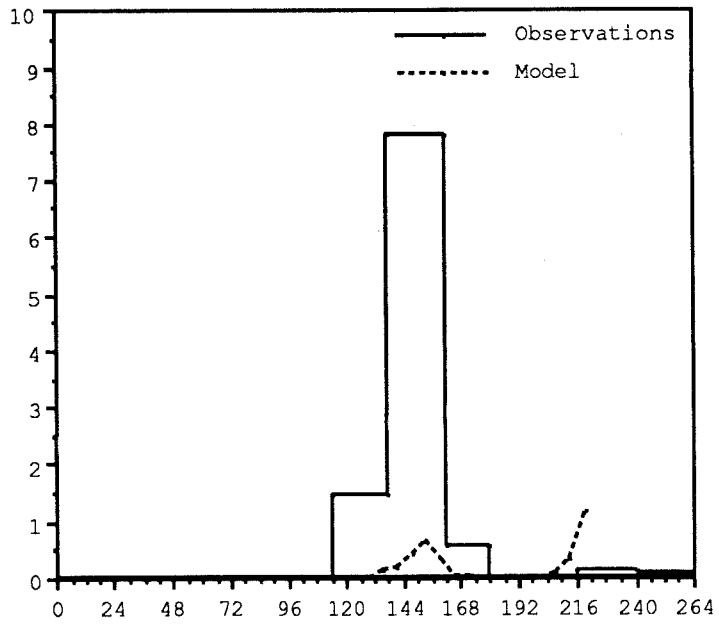

time (hours)

Bilthoven (NL)

Concentrations I-131
(Bq/m3)

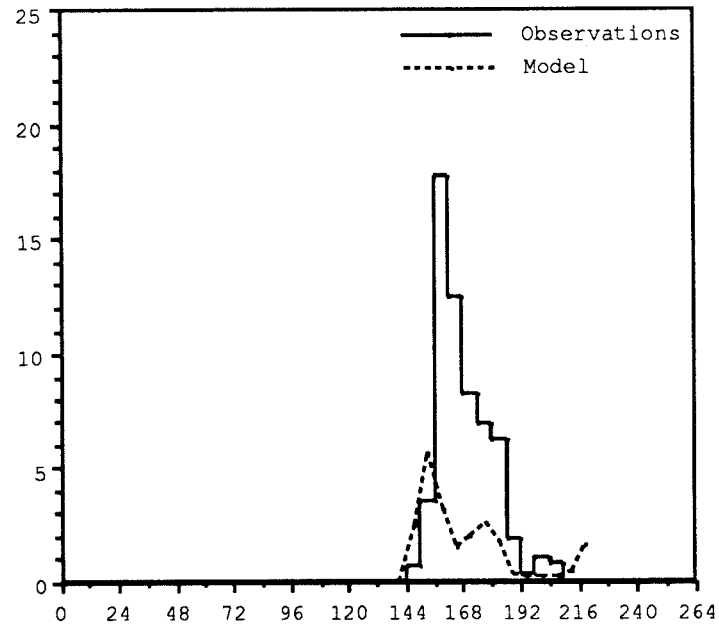

time (hours)

Braunschweig (FRG)

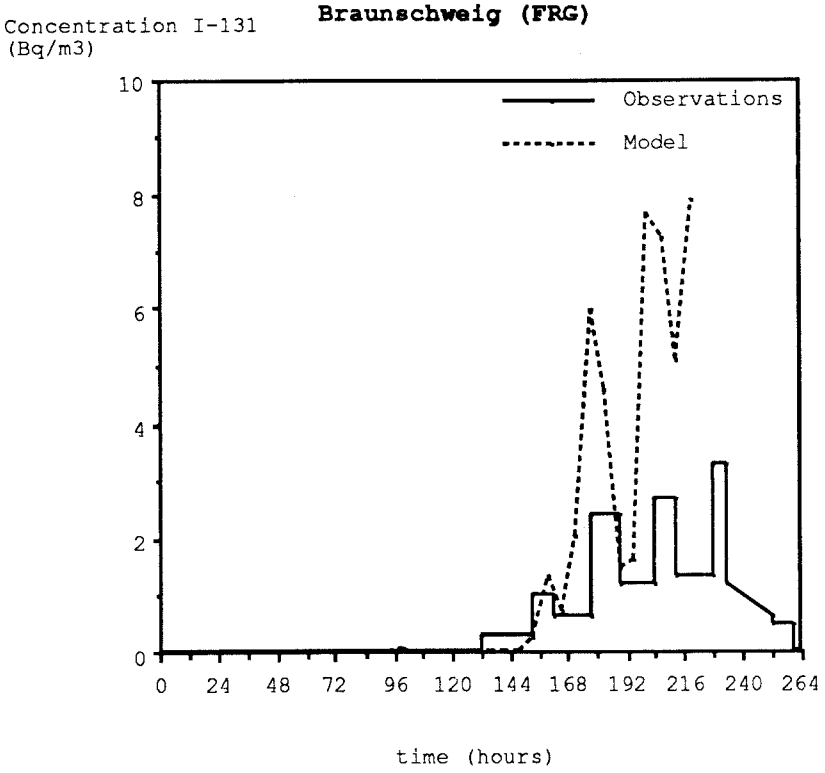

Varese (I)

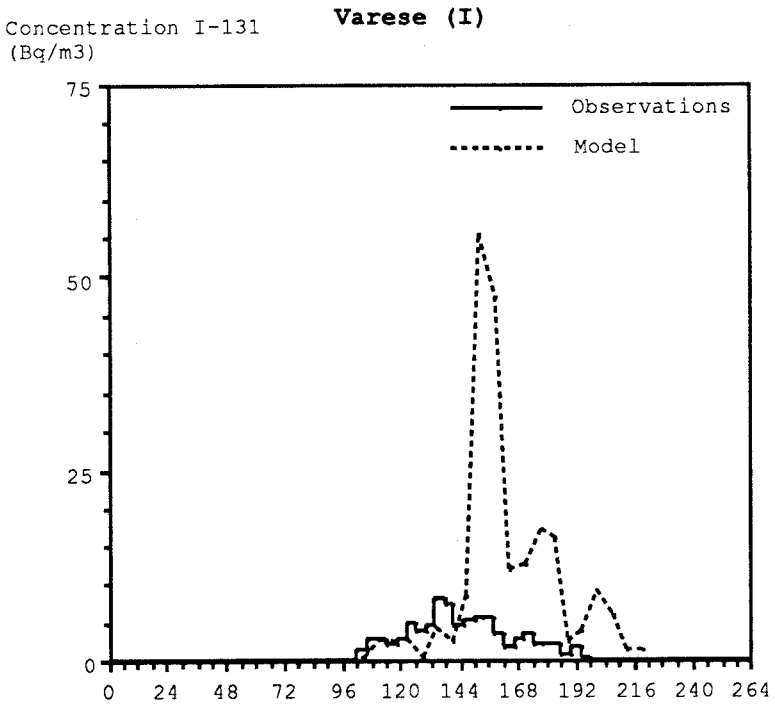

Marcoule (F)

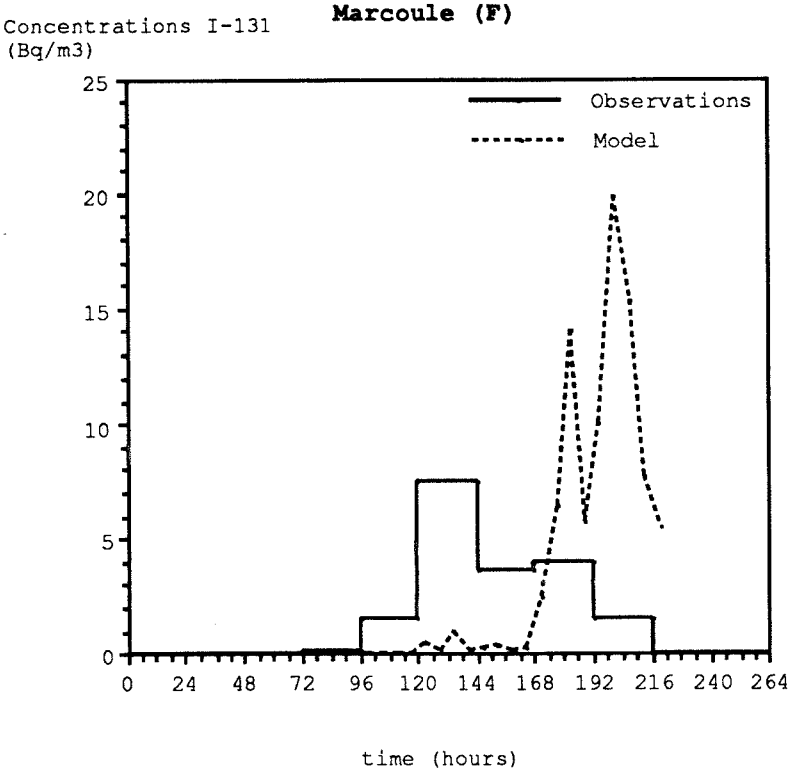

Harwell (UK)

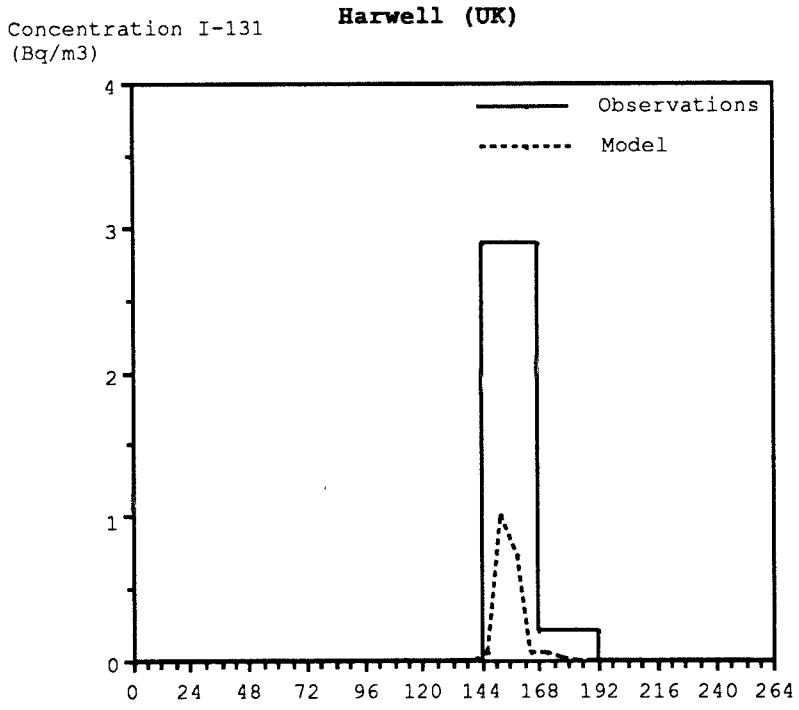

Symbols and notation

Bq	Bequerel; unit of radioactivity; number of desintegrations per second	
c	Concentration	(em.u.m^{-3})
<c>	Mean concentration in the fully mixed boundary layer	(em.u.m^{-3})
c' , c"	Constants	
C_p	Specific heat at constant pressure	($Jkg^{-1}K^{-1}$)
d	Thickness of one of the model layers	(m)
f	Coreolis parameter	(s^{-1})
g	Acceleration of gravity	(m^2s^{-1})
h	Mean height of the turbulent boundary layer	(m)
h_c	Mean height of the convective boundary l.	(m)
H	Effective source height	(m)
	also surface sensible heat flux density	(Wm^{-2})
I	Precipitation intensity	(mh^{-1})
k	Von Kármán constant	
K	Radioactive or chemical decay rate	(s^{-1})
K_z	Eddy diffusivity	(m^2s^{-1})
L	Obukhov length scale	(m)
ML	Mixed layer	
M_{ML}	Mixed layer mass of the puff	(em.un.)
M_{RL}	Reservoir layer mass of the puff	(em.un.)
p	Power of the 'power law' for wind profiles	
R	Total accumulated precipitation amount	(m)
r_a	Aerodynamic resistance	(sm^{-1})
r_b	Sublayer resistance	(sm^{-1})
r_c	Surface resistance	(sm^{-1})
RL	Reservoir layer	
R_L	Lagrangian autocorrelation function	
t	Time	(s)
t_{Lh}	Lagrangian timescale of horizontal velocities	(s)
t_{Lv}	Lagrangian timescale of vertical velocities	(s)

t_*	Characteristic timescale of subgrid horizontal diffusion	(s)
T	Air temperature	(K)
u_*	Friction velocity	(ms^{-1})
$\overline{u_p}, \overline{v_p}$	Time averaged wind speed in the x and y direction at the mass-centre of the puff	(ms^{-1})
$\vec{u}$	Time averaged wind vector	(ms^{-1})
Vg	Dry deposition velocity	(ms^{-1})
w_e	Entrainment velocity	(ms^{-1})
$\overline{w_h}$	Average vertical velocity at z=h	(ms^{-1})
x,y	Horizontal coordinates relative to the mass-centre of the puff	(m)
z0	Roughness length for momentum	(m)
$z0_c$	Roughness length for transport of gases	(m)
z_p	Height of the mass-centre of the puff	(m)
α	(modified) Priestley-Taylor parameter	
ϕ_m	Stability correction function for momentum	
ϕ_h	Stability correction function for heat	
Φ_m	Integrated stability correction function for momentum	
Φ_h	Integrated stability correction function for heat	
Λ	Scavenging coefficient	(s^{-1})
ξ	Scavenging ratio	
ρ	Density of the air	(kgm^{-3})
σ_r	Horizontal dispersion coefficient	(m)
σ_x	Dispersion coefficient in the alongwind direction	(m)
σ_y	Dispersion coefficient in the crosswind direction	(m)
σ_z	Vertical dispersion coefficient	(m)
σ	Vertical coordinate ($P/P_{surface}$; P=pressure)	

References

CCRX, 1988, Rapportage aanvullend meetprogramma Tsjernobyl CCRX-rapport (in Dutch), Ministerie van Volkshuisvesting, Ruimtelijke Ordening en Milieubeheer, 's Gravenhage.

Csanady, G. T. 1973. Turbulent diffusion in the environment. Dordrecht, Holland: Reidel publ. comp.

Dyer, A. J. 1974. A review of flux-profile relationships.Boundary-layer Met. 7,363-372.

ECMWF. 1987. User guide to ECMWF products.Reading,U.K.

Egmond, N. D. Van and H. Kesseboom. 1983. Mesoscale air pollution dispersion models II; Lagrangian PUFF-model, and comparison with eularian GRID model.Atmos. Environ. 17,265-274.

Egmond, N. D. Van, D. Onderdelinden and H. Kesseboom. Correlation spectrometry as a tool for mesoscale air pollution modelling. 13th International Technical Meeting on Air Pollution modelling and its Application, Iles de Embiez, France, 14-17 september 1982, Publ. Plenum Press, 1984.

Gifford, F. A. 1985. Atmospheric diffusion in the range 20 to 2000 kilometers. Air pollution modelling and its application V, St. Louis Missouri, USA, april 15-19, 1985., London, Plenum Press.

Gifford, F. A. 1977. Tropospheric relative diffusion observations.J. Appl. Met. 16,311-313.

Golder, D. 1972. Relations among stability parameters in the surface layer.Boundary-layer Met. 3,47-58.

Hanna, S. R. 1986. Lateral dispersion from tall stacks.J. Clim. Appl. Met. 25,1426-1433.

Holtslag, A. A. M. and H. A. R. De Bruin. 1988. Applied modelling of the nighttime surface energy balance over land.J. Appl. Met. 27,689-704.

Holtslag, A. A. M. and R. Van Westrhenen. 1989. Derivation of boundary-layer parameters from the outputs of atmospheric models.KNMI Scientific report WR 89-04,De Bilt, The Netherlands.

Leeuw, F. A. A.M. De, R. M. Van Aalst, H. J. Van Rheineck Leyssius, H. Kesseboom, N. D. Van Egmond, M. P. Scheele, H. Van Dop and A. P. Van Ulden. 1986. The Chernobyl accident: model calculations of concentration and deposition of radioactive releases.Paper submitted to the expert meeting on the assesment of the radioactive dose commitment in Europe due to the Chernobyl accident, RIVM, Bilthoven, The Netherlands, June 25-27

Louis, J. F. 1982. ECMWF forecast model; documentation manual Vol.1: Theoretical basis, Reading, U.K.

McNider, R. T. 1988. Influence of diurnal and inertial boundary-layer oscillations on long-range dispersion.Atmos. Environ. 22:2445-2462.

Nieuwstadt, F. T. M. 1981. The steady-state height and resistance laws of the nocturnal boundary layer: theory compared with Cabauw observations.Boundary-layer Met. 20,3-17.

OECD, 1987, The radiological impact of the Chernobyl accident in OECD countries,Paris..

Pasquill, F. 1974. Atmospheric diffusion. 2nd edition. Clichester England: John Wiley and Sons.

Pasquill, F. and Smith, F. B. 1983. Atmospheric Diffusion. Ellis 3rd ed. Horwood Ltd.
RIVM. 1990. The national air quality monitoring network; Technical description.RIVM technical report 228702017, RIVM, Bilthoven The Netherlands.
Saffman, P. G. 1962. The effect of wind shear on horizontal spread from an instantaneous ground source.Quart. J. R. Met. Soc. 88,382-393.
Smith, F. B. 1965. The role of wind shear in horizontal diffusion of ambient particles.Quart. J. R. Met. Soc. 91,318-329.
Smith, F. B. and M. J. Clark. 1989. The transport and deposition of airborne debris from the Chernobyl nuclear power plant accident with special emhasis on the consequences to the United Kingdom, scientific paper 42, MET Office, Bracknell..
Troen, I. and L. Mahrt. 1986. A simple model of the atmospheric boundary layer: sensitivity to surface evaporation.Boundary-layer Met. 37,129-148.
Turner, D. B. Workbook of atmospheric dispersion estimates.Office of air programs pub. No.999-AP-26, Public Health Service, Cincinnati, Ohio, 1969.
Ulden, A. P. Van and A. A. M. Holtslag. 1985. Estimation of atmospheric boundary layer parameters for diffusion applications.J. Clim. Appl. Met. 24,1196-1207.
Venkatram, A. 1988. An interpretation of Taylor's statistical analyses of particle dispersion.Atmos. Environ. 22,: 865-868.
Verver, G. H. L. and M. P. Scheele. Influence of non-uniform mixing heights on dispersion simulations following the Chernobyl accident. 17th International Meeting on Air Pollution Modelling and its Application, Cambridge, U.K., 19-22 september, 1988.,Plenum Publ. 1989.
Voldner, E. C., L. A. Barrif and A. Sirois. 1986. A literature review of dry deposition of oxides of sulphur and nitrogen with emphases on long-range transport modelling in North America.Atmos. Environ. 20,(11):2101-2123.
Wesely, M. L. and B. B. Hicks. 1977. Some factors that affect the deposition rates of sulphur dioxide and similar gases on vegetation.J. Air Pollut. Control Ass. 27,1110-1116.